Miltscho Andreev, BSc

Investigation of two fluorophores dissolved in predefined solvents with the goal to perform FRET by observing fluorescence.

Master's Thesis

to achieve the university degree of

Master of Science

Master's degree programme: Technical Physics

submitted to

Graz University of Technology

Supervisor

Schennach, Robert, Ao.Univ.-Prof. Mag. Dr.rer.nat.

Institute of Solid State Physics

Co-supervisor

Urstöger, Georg Johann, Dipl.-Ing. BSc

Graz, March 2018

Affidavit

I declare that I have authored this thesis independently, that I have not used other than the declared sources/resources, and that I have explicitly indicated all material which has been quoted either literally or by content from the sources used. The text document uploaded to TUGRAZonline is identical to the present master's thesis.

———————————————
Date

————————————————————
Signature

Acknowledgment

At this point I would like to take the opportunity to express my gratitude and appreciate people, who supported me completing this work.

First of all, I would like to thank my supervisor Robert Schennach for giving me the opportunity to work on this research project. His useful critiques and professional advice helped me breaking down problems into the essential issues.

Second, I would like to thank my co-supervisor Georg Urstöger for his guidance and valuable support. Whenever it was relevant and appropriate he supervised and encouraged me enthusiastically. Thereby, a lot of inspiring and constructive discussions were conducted during breaks.

Further, I want to thank Günther Leising for consulting me in the beginning of my work. My grateful thanks go to Olivia Kettner, who always offered me a helping hand in the laboratory and always had time for short, pleasant chats. Advice given by Ulrich Hirn has been a great help in improving my operation method and soft-skills.

I would also like to extend my thanks to the technical staff at the department of Solid state physics. Special thanks should be given to Harald Kerschbaumer and Birgit Kunert for providing me with the needed technical resources. I am particularly grateful for the assistance given by Elisabeth Stern, Esther Schennach, Claudia Bäumel and Kerstin Schefzik helping me out with the bureaucratic and administrative hurdles.

Abstract

Förster Resonant Energy Transfer (FRET) is a well-known research method in fields including medicine, chemistry and biology. Based on a dipole-dipole coupling between 2 fluorophores, defined as donor (D) and acceptor (A), the molecule interactions serve as a "spectroscopic ruler". It is a common technique applied for example to monitor distances of chemical reactions, molecule structural elucidations or in vivo cellular analysis.

The main target of this diploma thesis was to investigate the possibility of FRET between 2 predefined fluorophores dissolved in Dimethylformamide (DMF) and distilled water at pH 9 by recording their fluorescent response to an external irradiation in a spectrophotometer and a spectrofluorophotometer. For this purpose, the Förster distance and the FRET efficiency were introduced as figures of merit to illustrate the performance of the set-up. Based on preliminary assumptions, such as the negative impact of DMF on fiber-fiber linkage behavior, distilled water at pH 9 was prioritized in the course of research. Several concentration series were prepared in the range of a few micromole per liters up to the saturation concentration of the pure fluorophore solutions. Additionally, D-A mixtures were produced to obtain reference spectra and later calculate the Donor quenching and Acceptor sensitization. As a result of the assessment process, the Förster distance was determined to 4.4 nm and the FRET efficiency was calculated depending on the fluorophore concentrations.

The challenge of the research was the lack of information about the performance of the fluorophore interaction within the chosen environment

as a function of the concentration. Low concentrations did not yield into a conclusive FRET efficiency, since donor quenching was recorded, but no acceptor sensitization. Finally, extra fluorescence measurements were performed with a self-assembled set-up, avoiding inner filtering effects at relatively high concentrations (around 0.05 $\frac{mmol}{l}$) with a standard quartz glass cuvette. On the basis of this work distilled water at pH 9 is not a recommended solvent for this predefined fluorophore pair.

In the course of this research, 3 factors emerged to have a major impact on the functionality of FRET: 1st the fluorophore molecular structure, 2nd the compatibility of the solvents used and 3rd the solute concentrations.

Kurzfassung

Der Förster Resonanz Energie Transfer (FRET) ist eine bekannte Untersuchungsmethode und wird in verschiedenen Bereichen wie etwa in der Medizin, Chemie oder Biologie verwendet. Sie basiert auf Dipol-Dipol-Wechselwirkungen zwischen 2 Fluorophoren, welche als Donor (D) und Akzeptor (A) definiert sind. Diese Wechselwirkung kann als spektroskopischer „Maßstab" fungieren, mit dessen Hilfe chemische Reaktionen, molekulare Strukturen sowie in-vivo Untersuchungen an organischen Zellen überwacht werden können.

Das Ziel dieser Diplomarbeit bestand darin, herauszufinden, ob 2 vordefinierte Fluorophore, welche entweder in Dimethylformamid (DMF) oder in destilliertem Wasser mit dem pH-Wert 9 gelöst, das Kriterium eines Förster Resonanten Energie Transfers erfüllen. Hierfür wurde die Fluoreszenz der gelösten Fluorophore nach einer externen, elektromagnetischen Anregung mit einem Spektrophotometer sowie einem Spektrofluorophotometer untersucht. Der Förster-Abstand und die FRET-Effizienz wurden als Gütezahlen definiert, um das Verhalten des Aufbaus zu beurteilen. Basierend auf vorläufigen Prämissen, wie etwa dem negativen Einfluss des DMF auf Zellulose–Faser–Faser–Bindungen, wurde destilliertes Wasser mit pH 9 für die Forschungsarbeit ausgewählt. Hierfür wurden Konzentrationsserien beider Fluorophore in dem Bereich einiger Mikromol bis hin zu der Sättigungskonzentration der reinen Fluorophore im Lösungsmittel erzeugt. Zusätzlich wurden D-A Gemische produziert, um Referenzspektra zu erhalten, sodass in weiterer Folge das "Donor quenching" und die

"Acceptor sensitization" berechnet werden konnten. Folglich wurden der Förster-Abstand zu 4.4 nm und die FRET-Effizienz in Abhängigkeit der Konzentration bestimmt. Die Herausforderung dieser Arbeit war die mangelnde Information über das Verhalten der Fluorophore in der definierten Umgebung. Niedrige Konzentrationen ließen keine plausiblen Schlussfolgerungen zu der FRET-Effizienz zu, da zwar Donor–Intensitätsauslöschungen beobachtet werden konnten, jedoch keine Sensibilisierungen an Stelle des Akzeptors. Zum Schluss dieser Arbeit wurden weiterführende Fluoreszenzmessungen mit einem eigenen Aufbau durchgeführt, um Wechselwirkungsvolumen bedingte Filtereffekte zu vermeiden, die mit der Standard–Quarz–Küvette bei hohen Konzentrationen (0.05 $\frac{mmol}{l}$) auftraten. Aufgrund der Auswertungen im Rahmen dieser Arbeit wird destilliertes Wasser als Lösungsmittel für dieses Fluorophor–Paar nicht empfohlen.

Im Zuge dieser Forschungsarbeit wurden 3 Faktoren identifiziert, die eine essentielle Rolle für FRET spielen: 1. die molekulare Struktur der Fluorophore, 2. die Kompatibilität des Lösungsmittels und 3. die Konzentration der gelösten Stoffe.

Contents

Contents

List of Figures

List of Figures

1 Introduction

[1], [2], The dawn of modern paper making, especially the paper manufacturing process, can be assigned to the Chinese in the early 2nd century AD. The arts roamed to Korea and Japan, where paper makers started to use hemp, bamboo and kelp as a new raw material rather than the bast of daphne plants. With the expansion of Buddhism, the demand for these manufactured products reached Central Asia. In the 11th century Damascus was established as the main paper supplier of Byzantium and parts of Europe. It is the historical merit of the Arabians which pushed the development and distribution of the enhanced paper making techniques to lands far-off. Finally, it was the Moors people who brought the paper making production to the west end of Europe, Spain, passing through Morocco. After initial difficulties of convincing the western population of using manufactured paper instead of parchment, Gutenberg encouraged the breakthrough with introducing printing with mechanical moving letters, in the middle of the 15th century. From then on a lot of specialists and scientists concentrated on improving the production process of paper making with cotton or linen textiles. A remarkable milestone was set by Gottlob Keller 1843, who invented the wood pulp process by introducing wood as a new raw material.

[1], [2], In the 19th and 20th century the process chain from the raw material extraction to the final product was further developed and improved. Ahead of it all, the automation by means of the arising computer technology. Besides a mechanical pulping process to extract fibers, paper makers developed also a chemical treatment of this ground wood pulp to get rid of

unwanted properties induced by lignin, one of the main 3 components of wooden cells. A very common chemical treatment process, kraft pulping, uses sodium hydroxide and sodium sulphide. The mechanical and chemical procedures were followed by a washing step, to remove excess material which could be reused in the process chain and moreover help the organic material to recover. Once the preliminary treatments were finished and the fibers optionally bleached the product ended up with a stock preparation. The anticipated result was - A white sheet of paper.

1.1 Cellulose – Bonds and structure

[3], [4], Following an increasing demand of consumers and industry on renewable, sustainable and biodegradable resources, cellulose is considered to be one of the most abundant raw materials on earth. It is a common organic polymer with an almost inexhaustible source for bio applicable and ecologically friendly products. As demonstrated by the huge amount of wood-based industries such as paper or textiles supplying natural cellulose-based materials (wood, cotton, hemp, etc.), wood remains an important source of raw material to obtain cellulose stock. Cellulose based derivatives, which are produced on an industrial scale are used for packing, storing, coating as well as for pharmaceuticals, foodstuffs and cosmetics, to mention just a few. The attraction to cellulose results from worldwide accessibility and the particular cellulose structure.

[3], [4], The molecular structure of cellulose is composed of repeating glucose units called anhydroglucose rings ($[C_6H_{10}O_5]n$) whereby the degrees of polymerization, n, depends on the origin of the source material as well as from the treatment and ranges between $10000\ to\ 15000$. These single iterating monomer rings are linked together through an oxygen covalently bonded to the C1, C4 respectively, forming a $\beta\ 1-4$ glucosidic bond defined as the

basis cellobiose, shown in figure 1.1. Each repeating unit has 3 hydroxyl groups, which contribute to the inter-chain as well as the intra-chain bonds, to form stabilized linkages, following a cellulose structure formation. C1 is oxidized, so it has reducing properties whereas the the free hydroxy group C4 is non-reducing, shown in figure 1.2.
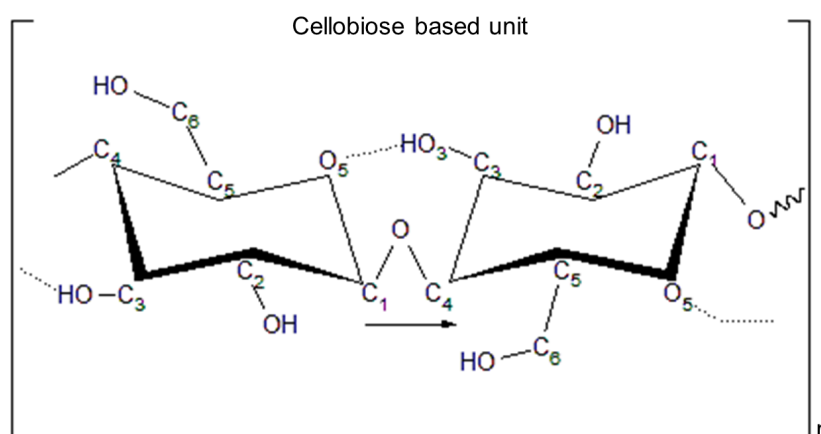
Figure 1.1: Schematic illustration of the cellulose structural conformation. Revised from [4].
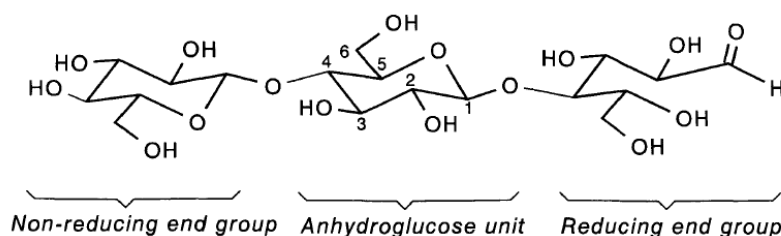
Figure 1.2: Schematics of the cellulose molecule structure. Revised from [4].

Physical-chemical interactions, such as van der Waals, hydrogen bondings and coulomb interactions can explain the high cohesive energy and the absence of a cellulose liquid state, illustrated exemplary later on in figure 1.3.

As a consequence, the reactions and subsequent properties of cellulose materials are determined by the chain lengths, chain distribution by the hydrogen bonds and the distribution of functional groups within cellulose chains and the pretreatment of the raw material.

1.1.1 Fiber-fiber interactions

[5], [6], Different mechanisms contribute to the cellulose fiber-fiber network bondings. While paper properties vary with fiber strength, network structure among the fibers as well as the fiber bonding and functional additives, 6 different effects and their interdependencies can not only provide insight into optimizing the papermaking process but also can open the door to future oriented materials based on cellulose: mechanical interlocking, inter-diffusion, hydrogen bondings, Van der Waals forces, Coulomb forces and capillary bridges, see figure 1.3.
The prerequisite of a fiber fiber conjunction is a molecular contact in the range of micro- and nanometres.
[5], [6], In the course of papermaking, fibers get mechanically and chemically treated. Water, as a key component, lets fibers swell. Single cellulose chains are able to diffuse from one fiber into a different one, described as interdiffusion. This effect not only affects the mechanical bond and serves as an fiber intercept. During the drying process **capillary forces** have an effect on the cellulose migration, by regulating the distance. Fibers get twisted and pinched into predefined shapes so they rearrange and adjust among each other with the result of **mechanical interlocking**. Since the surface is not smooth the parts sticking out of the fibers entangle each other.
Cellulose can either build **OH-bonds** within the same chain or branch to different molecules. The hydrogen bonding between $C5 - C3$ for example is an intra-molecular connection, depicted in figure 1.1. It is responsible for the chain stiffness. Whereas the OH-bond at $C6$ stacks vertically to another

cellulose chain and affects the molecular structure configuration.

[5], [6], **Van der Waals** forces are close ranged forces between atoms and molecules which can occur within temporary charge shifts between interacting bodies. Assuming the fiber textures consist of a surface roughness and the fiber fiber interface reach a nano-scale, Van der Waals forces become plausible.

The cellulose itself has no charged group, so coulomb interactions do not seem to be valid. However, including hemicellulose and external additives such as sodium (Na) or calcium (Ca), without going into detail, can form attractive **coulomb interactions** between each other.

| Hydrogen bonds | Mechanical interlocking | Dipole-Dipole interactions |
| Coulomb interactions | Capillary forces | Interdiffusion |
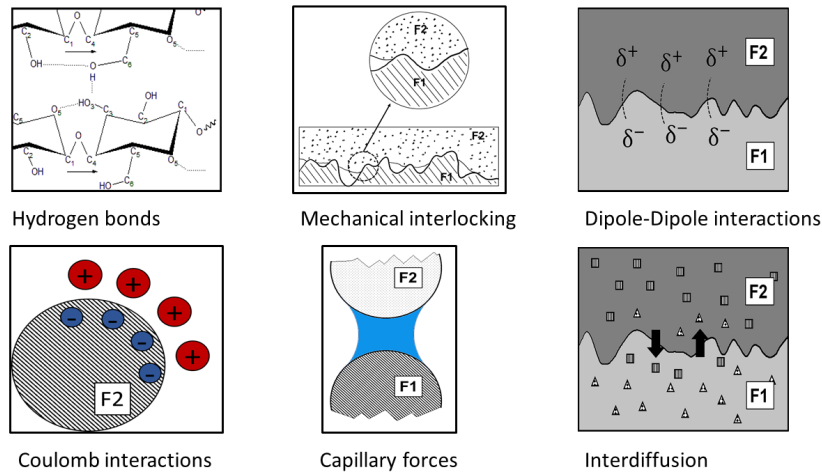
Figure 1.3: Schematics of the fiber-fiber bonding mechanisms of cellulose structures. Revised from [7].

1.2 Motivation

Paper. DIN A4. (210 *x* 290) *mm* - the final frontier. An omnipresent material. In the era of e-Business the use of paper based utilities is still a matter of course and an integral part of our everyday life. Products such as paper

sheets for printing, books, newspapers even organizers or household utensils like paper towels and toilet paper are indispensable. Invariable any country in the world uses banknotes as a means of payment. Although, a growing number of sectors tend to digitize information through adaptation with improving technology over time, people embrace this ordinary and common but innovative material.

These everyday used items in the sectors of industry such as packing paper, office or household have to fulfill different requirements in order to achieve its purpose. Starting from color, surface quality, chemical and mechanical resistivity up to the structural integrity or desired stress and strain behavior. Apart from pretreatments, additives can be chosen to vary the paper properties.

Although various properties of paper have already been studied, inter alia hydrogen expansion, recent investigations in the field of tensile strength of paper fibers demonstrate the complexity of fiber-fiber bonding mechanisms and the lack of exploration. Necessary for interactions between fibers is a molecular contact by a defined area with the help of which physisorption and the interdependencies of force effects such as Van der Waals, Coulomb interactions or mechanical interlocking can be explained.

At present, studies (of a research project team at Graz University of Technology) elaborate fiber-fiber conjunction investigations by Förster Resonant Energy Transfer (FRET), a non invasive, investigative method in order to define the molecular contact area. This resonant energy transmission depends on a dipole-dipole interaction between two fluorophore molecules defined as donor and acceptor, which are attached individually to the fibers. These chromophore molecules can be triggered by an incident light and coming close enough to each other, resonant energy can be transmitted from one fluorophore to the other. Fluorescence is one option, which can be observed as a result of the energy transmission. Current attempts of experimental implementation led to unsatisfying results without any evidence of insight into the molecular fiber contact, whereby the complexity of this research

field was revealed once again.

For this reason, it was necessary to change the investigation environment and introduce a more usable system: fluorophores dissolved in solutions examined in a standardized cuvette and defined volume.

1.3 Research objectives

This master thesis is elaborated in cooperation with the Christian Doppler Laboratory for fiber swelling and paper properties, which was formed to investigate the interrelationship of paper, pulp and fiber structures, as well as the chemical and physical fundamentals of fiber bonding mechanisms. Insight in this field of research could lead to a better understanding of paper strength and more over the control of cellulose conjunctions on a molecular level to get one step closer to an innovative, future-oriented material.

The aim of this master thesis is the development of an approach to simplify the investigation of the contact area cross-linked cellulose fibers by FRET as it is done in collaboration with the doctoral thesis of G. Urstoeger. It includes an empirical study of the solubility of predefined fluorophore molecules in different solvents and their absorbance and fluorescence behavior in various concentrations. Further on to investigate the possibility of a non radiative, resonant energy transmission by the method of FRET and illustrate the distance dependency in calculating the Förster radius. In the end the FRET efficiency, defined as a figure of merit, finalizes the applied method by giving insight into the performance of the fluorophore molecules in combination with the predetermined solvents.

The fluorophores used for this work were *7-(Diethylamino) coumarin-3-carbohydrazide* (DCCH) as the donor and *Fluorescein-5-thiosemicarbazide* (FTSC) as the acceptor molecule, which were provided from Santa Cruz Biotechnology (referring to section 2.3.2).

2 Fundamentals

This work is aiming at the target to offer a first approach to the subject of Resonance Energy Transfer (RET) between two predefined fluorophore molecules in a determined environment. The building blocks for the elaboration process were molecular spectroscopic methods and analysis tools to comprehend the investigated substances and study their behavior in dependence of their surrounding. Sources, which played an important role and influenced the author most, were the books *Principle of Fluorescence Spectroscopy*, *FRET - Förster Resonance Energy Transfer* and *Spektroskopische Methoden in der organischen Chemie*. They are cited with all additional contributions in the text at the beginning of each paragraph.

2.1 Molecular spectroscopy

Spectroscopy is a widespread field of different methods to analyze, identify and determine the molecular compounding of substances in the liquid, solid or gaseous state. All investigation methods are based on the interaction between matter and electromagnetic radiation to be used in physical chemistry. The response to electromagnetic radiation can reveal the chemical composition, monitor functional groups or explain the crystal structure of the investigated sample.

[8], Electromagnetic radiation is defined through the frequency ν or the wavelength λ, which are correlated to each other with

$$c = \nu \cdot \lambda \qquad (2.1)$$

and serves the equation of the photon energy

$$E = h\nu = \frac{hc}{\lambda} \qquad (2.2)$$

with the speed of light c (in vacuum $c \approx 2.99 \cdot 10^8 \ ms^{-1}$) and the Planck constant $h \approx 6.63 \cdot 10^{-34} \ Js$.

Depending on the energy E, outer shell electrons can be excited by a prior interaction of electromagnetic radiation with a molecule. Subsequently the energy gets absorbed in the respective range from ultraviolet upto visible light restricted by the wavelength range of around $(100 - 700) \ nm$, shown in figure 2.1, which illustrates the electromagnetic spectrum.

2.1.1 Absorbance and extinction coefficient

[9], However, the light absorption at a specific frequency of a molecule satisfies requirements, which should be considered inter alia:

1. the presence of a state ψ_0 at which the molecule can absorb the incident light with an eligible energy to be excited to ψ_1 and $E_1 - E_0 = h\nu$ exists.
2. the dipole moment μ_{01} is not equal to 0, although the condition $\Delta E = h\nu$ might be fulfilled.
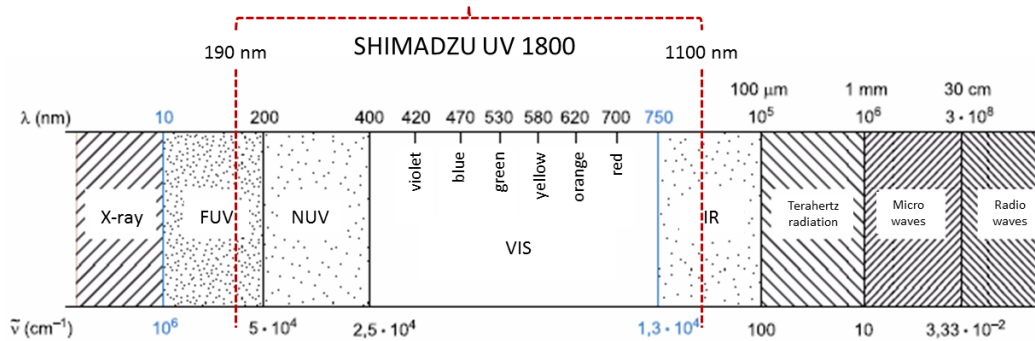
Figure 2.1: Schematics of the electromagnetic spectrum. Revised from [8].

Based on the Beer-Lambert-Bougeur law the absorbance (optical density) and the extinction coefficient can be determined.
[8], If light passes a homogeneous, isotropic substance with the thickness d its intensity I_0 gets lowered by absorption, neglecting scattering I_{sca} and reflection I_{ref} effects. The attenuated transmission intensity I is determined as:

$$I = I_0 - I_{abs} - I_{ref} - I_{sca} \tag{2.3}$$

Figure 2.2 depicts illustrative a cuvette from the side, investigated by a monochromatic light beam I_0 perpendicular to the vertical cuvette axis and parallel to its observation value I.
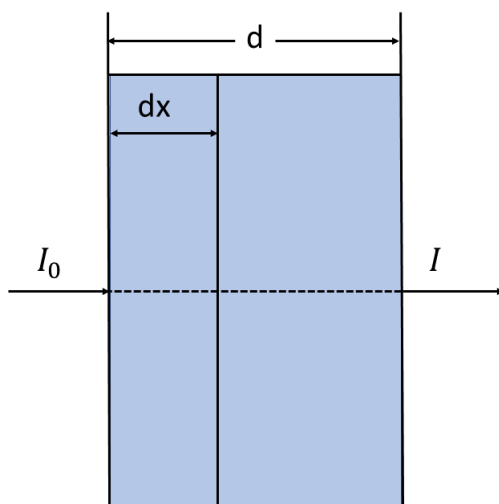
Figure 2.2: Schematics of the intesity transmittance through a homogeneous, isotropic substance. Revised from [8].

[8], Evaluating the differential ansatz with, the absorption coefficient α and the increment dx for the cuvette width,

$$\mathrm{d}I = -\alpha \cdot I \mathrm{d}x \tag{2.4}$$

the passing light equals

$$I = I_0 \cdot e^{-\alpha d} \tag{2.5}$$

In this case I determines the attenuated intensity in dependence of the thickness d^1 of the medium enclosed by the cuvette and its absorption coefficient α, depending on the molecular compound. Once the experimental

---

[1]d equals the diameter of the cuvette with a square base area

value I is defined, further relevant values in the absorption spectroscopy can be expressed such as the transmittance $T = \frac{I}{I_0}$, accordingly the absorption $1 - T$ and the absorbance, defined as the negative decadic logarithm of the transmittance. If dissolved agents in diluted solutions with the concentration c are investigated the expression can be rewritten, by replacing α with $2.303 \cdot \epsilon \cdot c$ and evaluating the natural logarithm of equation 2.5:

$$ln(T) = ln(\frac{I}{I_0}) = -2.303 \cdot \epsilon \cdot c \cdot d \tag{2.6}$$

to get to the absorbance $A(\lambda)$

$$A(\lambda) = -log(\frac{I}{I_0}) = \epsilon(\lambda) \cdot c \cdot d \tag{2.7}$$

[10], The absorbance $A(\lambda)$, also known as the optical density (OD), is dimensionless usually measured for a light path d of 1 *cm* (a standard cuvette) and the concentration of the sample c given in $mol \cdot l^{-1}$. The OD of the sample should neither be too low, causing errors after background correction, nor too high, to avoid sample saturation. A range of $(0.1 \; to \; 3.0)$ OD can provide satisfactory results.

In consequence to $A(\lambda)$ the molar extinction coefficient $\epsilon(\lambda)$ can be calculated and measures how strongly a dissolved substance attenuates the incident light and is given in $l \cdot cm^{-1} \cdot mol^{-1}$.

$$\epsilon(\lambda) = \frac{A(\lambda)}{c \cdot d} \tag{2.8}$$

Due to the difference of possible electronic state transitions, the spectrum is streaked with various bands, which can be distinguished by position, intensity and shape.

[9], Figure 2.3 illustrates schematically the absorption and emission spectra evolution of vibronic level transitions depending on the molecular structural complexity. With increasing number of atoms the number of possible vibronic energy transitions rises. Absorption and emission spectra, commencing with a discrete vibronic level transition start to blur with growing structural molecular complexity. Spectra of more convoluted molecules become continuous upto a smooth shape without any structural information of the molecule.
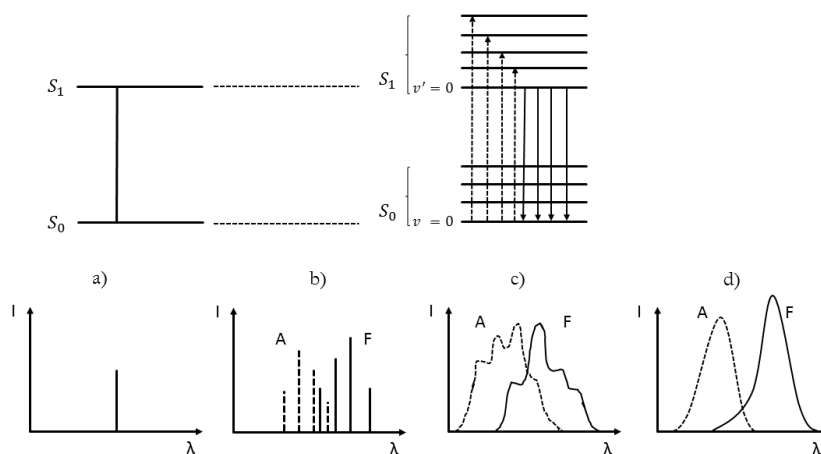
Figure 2.3: Schematics of absorption and emission spectra illustrated of vibronic level transitions, (a) atoms, (b) ordinary- (c) more complex- (d) complex molecules. Revised from [9].

2.1.2 Luminescence

[11], Luminescence is an observed phenomenon of electromagnetic radiation, which results in light emission of electronically excited substances. Formally luminescence can be categorized into two different categories - fluorescence and phosphorescence - depending on the relaxation from the excited state to a lower one, whether singlet or triplet transition.

Fluorescence

[11], Fluorescence is defined as the transition of an excited singlet state of an electron, in an excited orbital, paired to its counterpart in the ground state with opposite spin. In consequence the relaxation is allowed and occurs by an emission of a photon at a rate of typically $10^8 \ s^{-1}$ and a corresponding fluorescence lifetime of 10 ns.

Some common fluorophores are shown in figure 2.4 and as pictured, they are generally aromatic molecules. Quinine for example, present in tonic water and known from the widely encountered cocktail "Gin Tonic", is responsible for a faint blue glow on the surface of this drink.
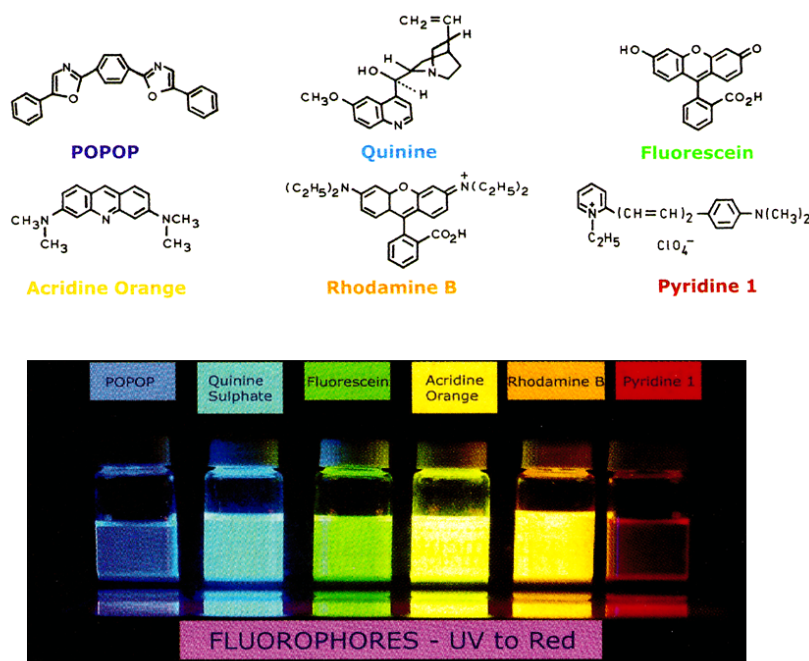
Figure 2.4: Common fluorophores used for fluorescence spectroscopy. Revised from [11].

Conventionally, fluorescence spectra are depicted as emission spectra originating from the fluorescence intensity plotted over wavelength or wave number, sometimes in combination with the excitation (absorption) spectrum shown in figure 2.5. The excitation spectrum of quinine shows 2 excitation peaks, but just 1 emission peak. This phenomenon can be explained by excitation into the 1_{st} and 2_{nd} singlet state, internal conversions and emission from the lowest excited state.

Figure 2.6 illustrates exemplarily the interrelationship between the molecular structure, the spectral properties and the energy transitions.
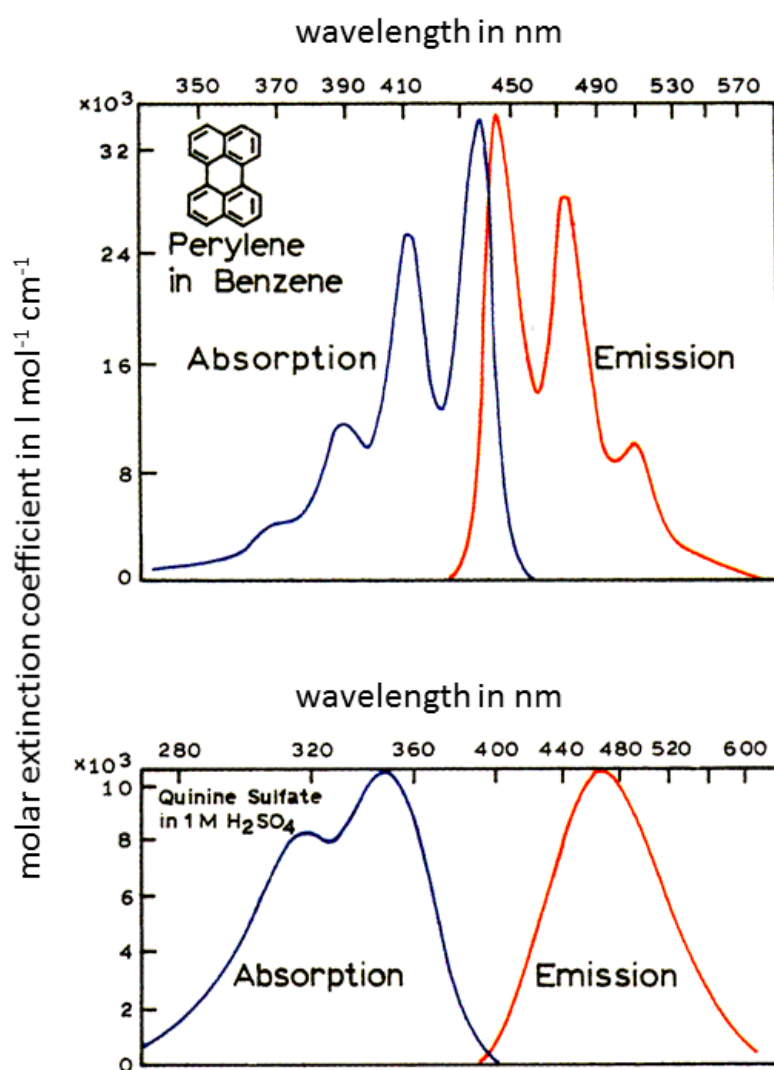
Figure 2.5: Absorption and emission spectra of perylene and quinine. Revised from [11].
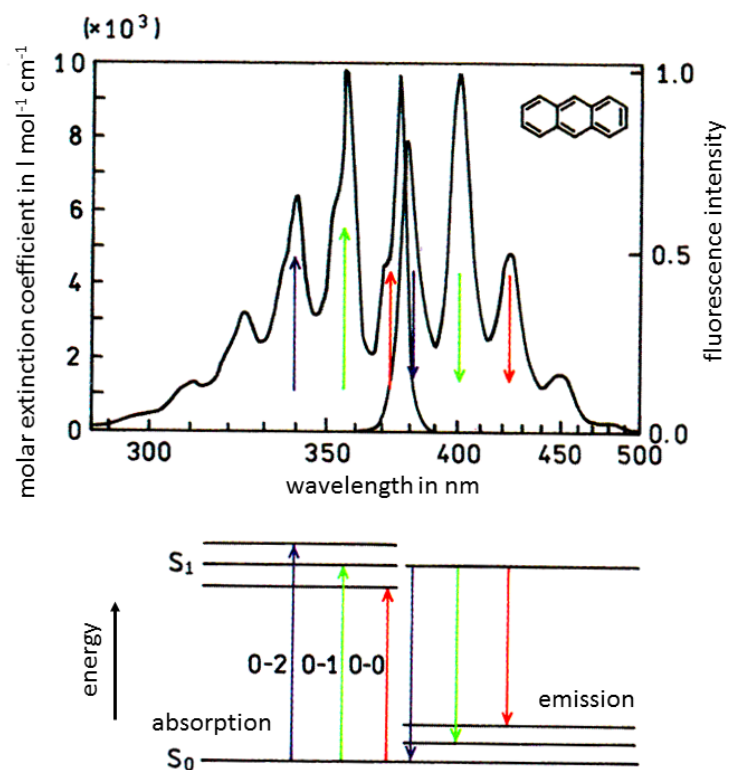
Figure 2.6: Absorption and emission spectra of anthracene with schematics of energy transitions. Revised from [11].

Phosphorescence

[11], Vice versa, phosphorescence is the emission of light from excited triplet states, undergoing a spin conversion from S_1 to T_1, called intersystem crossings, see figure 2.7. Thus, an electron coming from the excited orbital has the same spin orientation as the one returning to in the ground state. ($T_1 \rightarrow S_0$ can also happen through a non-radiative intersystem crossing process.) The relaxations from the triplet T_1 to the singlet ground state S_0 are quantum mechanically forbidden. As a result, in comparison to the fluorescence, the emission rates are several orders of magnitude smaller and thus slower $(10^3 \ to \ 10^0) \ s^{-1}$ with a phosphorescence lifetime upto 1 second, known from the "glow-in-the-dark" toys with even longer lifetimes. Consequently, phosphorous substances glow for a few minutes, following the exposure to light.

Depending on the structure of the molecule, both fluorescence as well as phosphorescence can be emitted, which makes it challenging to distinguish between them.
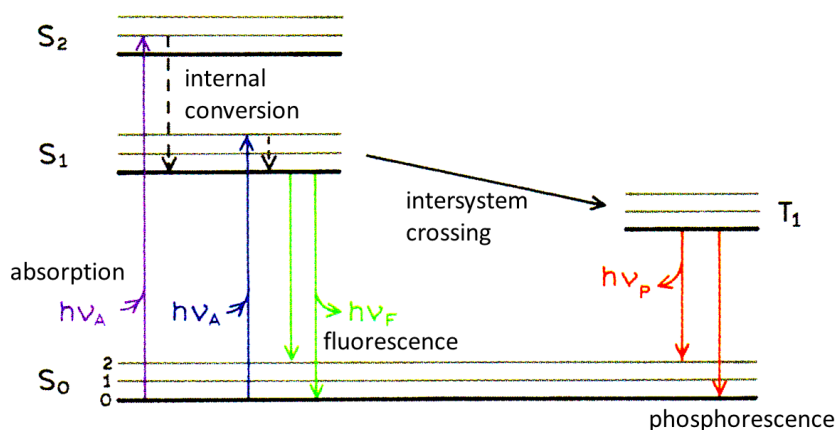
Figure 2.7: Schematics of a simple jablonski diagram. Revised from [11].

Jablonski diagram

[11], Jablonski diagrams are used to illustrate different processes that can occur once a molecule gets excited, id est, absorption as well as emission of light and possible actions in between, such as quenching, energy transfer or solvent influenced shifts, exemplarily shown in figure 2.7. Unlike an atom, a molecule consists of additionally more electronic transitions through the vibrational and rotational motion.

S_0 to S_2 and T_1 display the singlet and the triplet electronic state, with suggested vibrational energy levels, enumerated by 0,1,2, respectively. Following the absorption of electromagnetic radiation, a fluorophore can be excited to a vibrational level of either S_1 or S_2. Through internal conversions, a non-radiative transition, the molecule reaches a thermally equilibrated excited state, the lowest vibrational state of S_1 - so it dissipates energy into heat. From this excited state the electron can return to different energetic vibrational ground state levels, whereof the emission vibrational band structure arises. In consequence the emission spectrum can be thought theoretically, as a mirror image of the absorption spectrum of the states $S_0 \rightarrow S_1$, see figure 2.5, top.

The bottom spectrum of figure 2.5 shows a counterexample with the absorption maxima at around 315 and 340 nm, caused by excitation to the 1_{st} and 2_{nd} excited state with following relaxation into S_1. As supplied before, emission transitions occur predominantly from the lowest vibrational singlet state, in this case at around 460 nm. So in this case the emission spectrum is a mirror-image of the $S_0 \rightarrow S_1$ absorption. Another example, figure 2.6, shows, besides the 2 accompanying measured spectra of anthracene (a polycyclic aromatic hydrocarbon), a schematics of possible absorption and emission transitions. However, in the majority of cases the mirror-image rule is an exception. Hence, the absorption as well as the emission bands depend on the energy extent of the electronic transition.

[11], The rapid thermalization step from higher energetic levels to the lowest

vibrational state in S_1, by dissipating excess energy (into heat), points out the emission spectra independence of the excitation wavelength, as long as absorption is possible. Hence, fluorescence emission spectra, more precisely their shape and correspondingly the band structure, can be observed irrespectively of the excitation wavelength, kept in mind, that the intensity will change.

The electronic transition energy can be defined as an interplay of the electronic vibrational and rotational molecular states:

$$\Delta E_{tot} = \Delta E_{elec.} + \Delta E_{vib.} + \Delta E_{rot.} \tag{2.9}$$

Stokes shift

[11], Another interesting feature, the "Stokes shift", defines the energy loss between excitation and emission spectrum, universally observed for fluorescent molecules dissolved in solutions. Apart form the prior thermalization of excess vibrational energy into S_1 and further rapid decaying into vibrational energy levels in S_0, further common causes of the energy loss can be due to solvent effects linked to excited-state reactions and complex formation or energy transfer. Since the excited molecule can differ from its molecule part in the ground state, the Stokes shift can increase, in consequence of the influence of a polar solvent to the excited state S_1 and its theoretically greater dipole moment than S_0.

2.2 [F]RET

"Resonance energy transfer (also called FRET), the main topic of this book, is the radiationless transmission of an energy quantum from its site of absorption to the site of its utilization in a molecule, or system of molecules, by resonance interaction between chromophores, over distances considerably greater than interatomic without conversion to thermal energy and without the donor and acceptor coming into kinetic collision.[2]"

[8], [10], [11], FRET, an acronym for Förster[3] Resonant Energy Transfer, is a strongly distance-dependent transmission of energy between 2 fluorophores. The studied systems and objects of interest need to provide a distance of approximately $(20 - 90)$ Å so that energy transfer can take place.
[11], The most common metaphor used to explain resonance between two fluorophores is a coupled pendulum, introducing a spring connection between the 2 rods. When one pendulum starts to swing (the donor molecule absorbs radiation energy) the other part will continue swinging (the acceptor fluoresces). The theory is based on the concept of energy exchange between 2 dipoles with similar resonance frequency. Whereby radiative RET works due to absorption and emission of photons.
Provided that the system distance range is chosen correctly, an appropriate pair of molecules, indicated as donor (D) and acceptor (A), is required between which resonant energy transfer (RET) can take place. Taking particular attention to the distance dependency a few additional conditions need to be laid down to observe FRET:

---

[2] (10), ch.3 Förster Theory, p.33

[3] (10), ch.5 FRET-More than a Four-Letter Word!, p.105, The "F" in the acronym FRET can either stand for fluorescence, which is usually involved in such experiments. Another reason is to acknowledge Förster's work on spectroscopic data to energy transfer events.

The following key quantities essential in Förster's theory were used in this thesis:

Table 2.1: Essential key quantities in Förster's theory

#	variables	descriptions	units
1	r_{DA}	distance between D and A fluorophore	nm
2	R_0	distance r, at which FRET efficiency equals 50 %	nm
3	$\epsilon_A(\lambda)$[4]	extinction coefficient of acceptor molecule	$l \cdot mol^{-1}cm^{-1}$
4	J[5]	overlap integral of the D emission and A excitation	$l \cdot mol^{-1}cm^{-1}nm^4$
5	η_{RET}	energy transfer efficiency $\in [0,1]$	
6	$\kappa^2 = \frac{2}{3}$[6]	orientation factor between fluorophore dipoles $\in [0,4]$	
7	$\Phi_D = 0.184$[8]	quantum yield of D in absence of A $\in [0,1]$	
8	$n = 1.33$[10]	refractive index of fluorophores dissolved in solvent	

1. **Both, D and A must have a dominant electronic transition in the ultraviolet (UV), visible (VIS) and/or infra-red (IR) range.**
   Fluorophore molecules can be discussed on the basis of conjugated polymers. A polymer is a large repetitive molecule structure (referring to monomers and oligomers), which can be summarized by different

---

[4]$\epsilon_A(\lambda)$ is often given in units of $M^{-1}cm^{-1}$ or $lmol^{-1}cm^{-1}$

[5]J is often given in units of $M^{-1}cm^{-1}nm^4$

[6]The orientation factor was chosen with reservations.[7]

[8]The luminescence quantum yield of the donor was taken from the literature stating a similar donor molecule.[9]

[10]The refractive index was chosen to $n = 1.33$ to perform the calculations in aqueous solutions. The value can change by varying solvent, solute and concentration.

classes as homo- and copolymers. Whereas the structure can vary from planar monomer chains upto complex assembled olefines or rather polyenes. In contrast to atoms, molecular orbitals (MO) theory is used to classify the electronic transitions, illustrative mentioned through the transitions between MO such as σ or π to σ^* and π^* and vice versa.

If polymer structures contain isolated chromophore groups, functional attachments called auxochromes, with π and n orbitals, which do not interact with each other, an electronic transition, thus an absorption spectrum is likely to be observed. The auxochromic effect, yielding in a hypsochromic (to lower λ) or bathocromic (to higher λ) shift, is caused by a Lewis acid or base. Lewis bases for example (functional groups such as $-\overline{O}H$, $-\overline{O}R$, $-\overline{N}H_2$, $-\overline{N}R_2$ or $-\underline{\overline{S}}R$ et al.), donate free electrons to the chromophore with their n orbitals. Introduction of alkyl groups as well as multiple olefine double-bondings lead to a bathocromic shift, a shift to longer wavelengths by decreasing the energy gap between the highest occupied MO (HOMO) and the lowest unoccupied MO (LUMO).

The molecular structural composition of the most common organic fluorophores with extensive characterization of FRET properties are shown in figure 2.8.
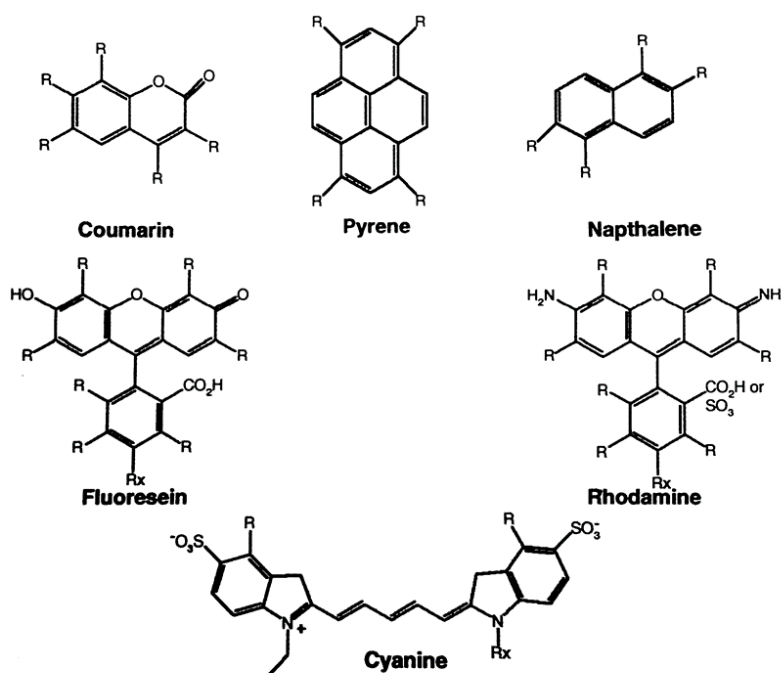
Figure 2.8: Common used organic dyes categories proven to have luminescent properties, commercial availability and an option for bio attachments. Revised from [11].

2. **Spectral overlap $J(\lambda)$ of D emission and A excitation spectra must exist (and has to be in the same wavelength rage).**

   [10], Charges bound in a molecule, similar to an atom, have quantized energy levels. RET, with the requirement of a non-radiative, resonant energy transmission is the result of a dipole-dipole long-range interaction between D and A. As mentioned above, the Jablonski diagram does not only apply for intramolecular but also for intermolecular transitions. So it is evident that once the D gets close enough to the A, transfer may take place from an excited D state in which the A state is not yet exited to transmit its energy to the A and induce an A excitation. Important to remember, RET is theoretically neither a process involving a D emission nor a reabsorption of a photon on the

part of the A.

$J(\lambda)$, defined as the overlap integral, expresses the extent of spectral overlap between the D emission and A excitation spectrum. $\bar{I}_D(\lambda)$ is dimensionless and in this case the corrected D fluorescence intensity with the total intensity normalized to unity. $\epsilon_A(\lambda)$ represents the molar extinction coefficient spectrum of the A molecule.

$$J(\lambda) = \int_0^\infty \bar{I}_D(\lambda)\epsilon_A(\lambda)\lambda^4 d\lambda \tag{2.10}$$

with

$$\int \bar{I}_D(\lambda)d\lambda = 1 \tag{2.11}$$

In figure 2.9 there are 3 different ordinate scales. The left scale represents the corrected D emission intensity, the right one is the calculated extinction coefficient spectrum of the A. The third one arises out of the convolution of the spectrum $\bar{I}_D$, the extinction coefficient spectrum $\epsilon_A(\lambda)$, with a weighting factor of λ to the power of 4. The zone with a gray background marks the possibility of a RET between the 2 fluorophores as depicted in figure 2.10. As long as there exists a spectral overlap of the D emission and the A excitation spectrum, which involves resonating energy levels of both species, an energy transfer is likely to take place. This process can be influenced by different sources of irritation, discussed on the following pages.
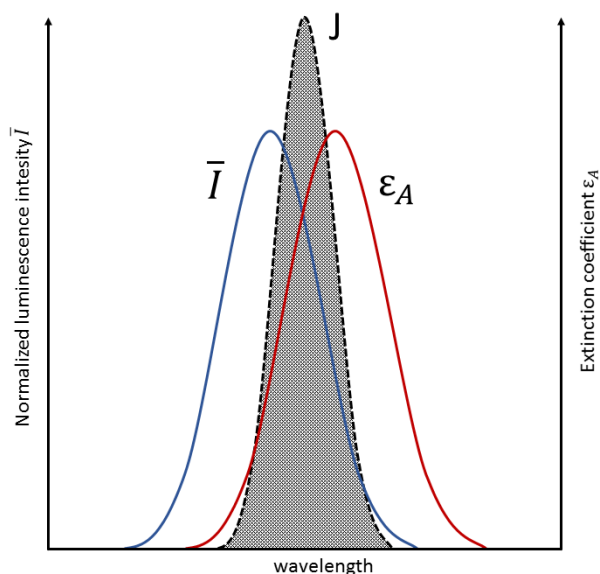
Figure 2.9: Schematics of the D emission $\bar{I}_D$ and A extinction $\epsilon_A(\lambda)$ spectra overlap. Revised from [10].
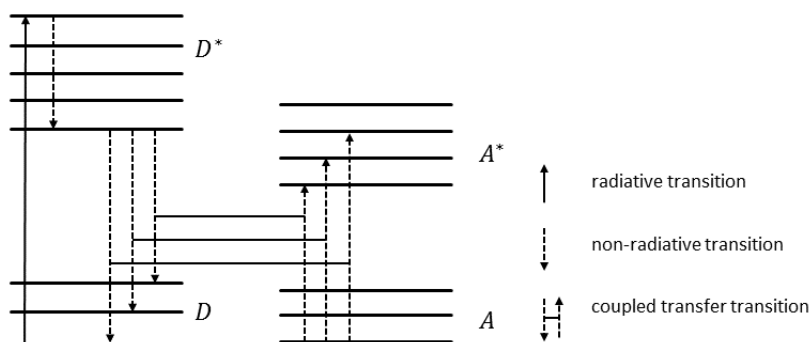
Figure 2.10: Schematics of a simplified jablonski diagram of RET. D^* and A^* denote excited states of the donor and acceptor molecules, respectively.

3. **Energy transfer rate $k_t(r)$ and the calculated FRET efficiency $\eta_{FRET}(r)$.** [10], [11], The energy transfer rate depends on the spectral overlap extent of the D emission spectrum with the excitation spectrum of

27

the A and other factors such as the distance between the D and A molecules, the relative orientation of the dipoles involved and the quantum yield of the D. Eventually, the distance dependency of RET is not only sufficient but necessary granting the possibility of displacement measurements between these two fluorophore molecule dyes. The rate of energy transfer allows the determination of a static or a time resolved separation among two macromolecule sites and is defined as

$$k_T(r) = \frac{1}{\tau_D} \left(\frac{R_0}{r} \right)^6 \tag{2.12}$$

where the decay time of D in absence of A is determined by τ_D, r is the distance between the D and A molecule (distance between two dipoles) and R_0 is the Förster distance, at which the RET is 50% efficient, a figure of merit in fluorescence spectroscopy.

[10], [11], Hence 2 important insights: First, the energy transfer rate $k_t(r)$ is equal to 50% at the distance $r = R_0$ and second, as a consequence, the decay rate of the donor emission decreases to its half intensity. Evidently, the RET depends strongly on $\frac{1}{r^6}$ and can be applied as a "spectroscopical ruler." (L. Stryer, 1978 [13]; Th. Förster, 1948 [14]). Consequently the FRET efficiency is determined as

$$\eta_{FRET}(r) = \frac{k_T(r)}{k_T(r) + \frac{1}{\tau_D}} = \frac{1}{1 + \left(\frac{r}{R_0} \right)^6} \tag{2.13}$$

which again illustrates the sensitivity of the RET to the distance between the D and A molecule, shown in figure 2.11.
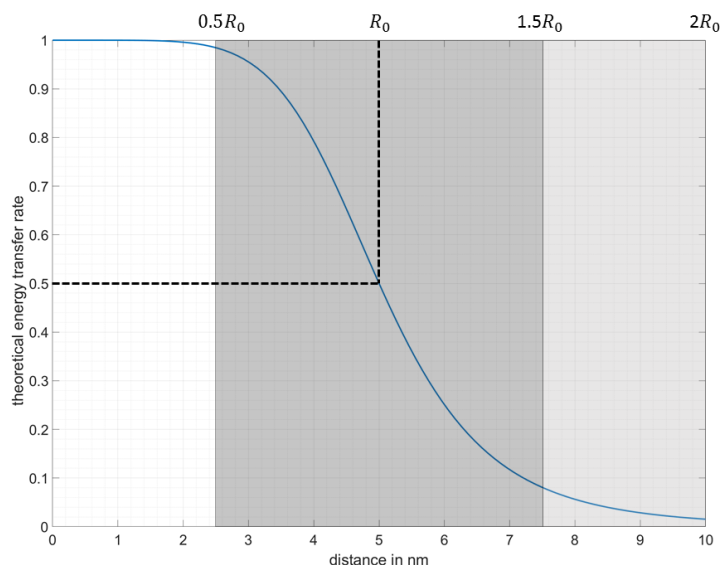
Figure 2.11: FRET efficiency η_{FRET} in dependency of the D-A distance r, which is very prominent in the range of $0.5R_0$ and $2.0R_0$ (with gray background). Revised from [10].

[10], In order to determine the scientific merit of the RET efficiency, which relates the interaction of the 2 fluorophore molecule dyes in dependence on their distance r, thus the Förster distance R_0, with spectroscopic data, 2 different methods were used in this master thesis:

a) **Donor quenching**
   One possibility to calculate $\eta_{FRET}(r)$ is to use the D emission intensity spectroscopic data in presence as well as in absence of the A (with the subscripts DA and D), I_{DA} and I_D, respectively.

$$\eta_{FRET}(r)_{DQ} = 1 - \frac{I_{DA}}{I_D} \tag{2.14}$$

b) **Acceptor sensitization**
   As the donor quenching can also be triggered by different deactivation effects (see section **6.**), than pure $D - A$ RET, the only

evidence to confirm energy transfer is to investigate the lumines-cence of the A following the excitation of the D. In almost all cases there is a direct excitation of the A when exciting the D, that needs to be taken into account.

$$\eta_{FRET}(r)_{AS} = \left(\frac{I_{AD}}{I_A} - 1 \right) \left(\frac{\epsilon_A}{\epsilon_D} \right) \tag{2.15}$$

Using the equations 2.14 and 2.15 with the a priori determined emission fluorescence intensities I_i are only valid, if the instruments parameters for the probe measurements were identical.

RET causes a donor fluorescence intensity quenching, resulting in a decrease of the emission intensity of the donor in presence of the acceptor I_{DA} compared to the pure donor emission signal I_D. Simultaneously the mixed acceptor emission I_{AD} is assumed to increase, displayed in figure 2.12. It shows a theoretical, qualitative constellation of D-A excitation and emission spectra relative to the measured fluorescence spectra including the overlap of both species. The arrows pointing up and down describe the emission evolution resulting from a D-A RET. However, neither the position nor the relative height of the intensity peaks correspond to real values and is intended for demonstration purpose only.
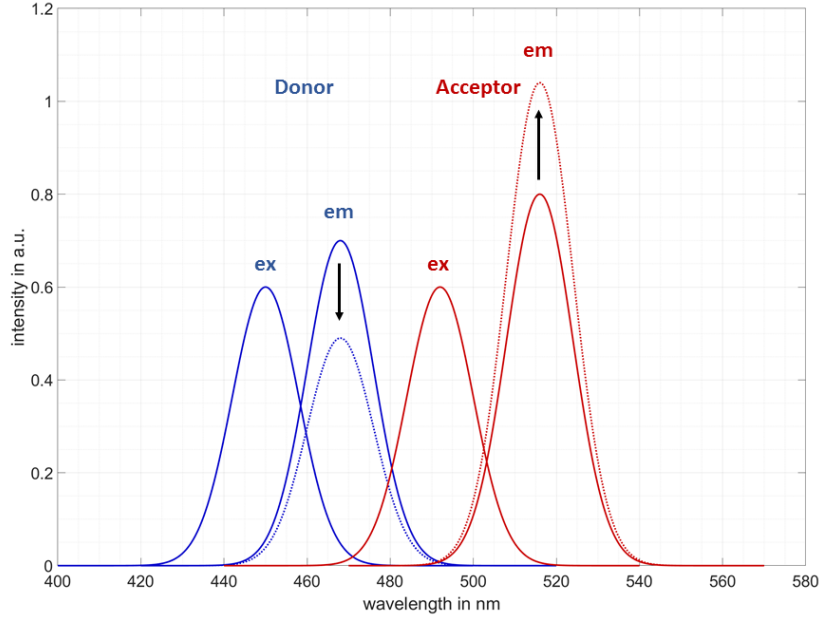
Figure 2.12: Theoretical excitation (ex) and emission (em) spectra of D and A molecule. The down- and upwards pointing arrows denote a de- and increase of the molecules emission intensity spectrum.

4. **The Förster distance** R_0.

Despite the fact that the Förster distance R_0 correlates to 50% of the energy transferred between the D and A, it is a material specific key figure (with respect to the fluorophore pair and the prescribed environment).

[10], [11], Referring to the review by Clegg (R.M. Clegg, 1996 [15]), a more sophisticated rate of transfer is given by

$$k_T(r) = \frac{\Phi_D \kappa^2}{\tau_D r^6} \left(\frac{9(ln10)}{128\pi^5 N n^4} \right) \int_0^\infty \bar{I}_D(\lambda) \epsilon_A(\lambda) \lambda^4 d\lambda \qquad (2.16)$$

where the integral illustrates the overlap integral $J(\lambda)$ derived above, Φ_D is the quantum yield of the D molecule in absence of the A, κ^2

is the orientation factor, τ_D is the D lifetime in absence of A, r is the distance between the two fluorophore molecules, N is the Avogadro's constant and n is the refractive index (assumed to be $n = 1.33$). [10], [11], Once the rate of transfer is derived, it is more common to rewrite the formula in terms of the Förster distance R_0, at which distance, half of the D energy transfers non-radiative to the A and half of the energy decays by other radiative and non-radiative effects. From eq. 2.16 and eq. 2.12 the Förster distance R_0 is obtained with $k_T(r) = \frac{1}{\tau_D}$.

$$R_0 = \frac{\Phi_D \kappa^2 9 (ln10)}{128\pi^5 N n^4} J(\lambda) \tag{2.17}$$

5. **The quantum yield of the D emission should be arguable high and the orientation factor κ^2 equals 2/3.**

[10], [11] The quantum yield Φ, especially Φ_D is a figure of merit, which quantifies the ratio between the number of emitted photons and the number of absorbed photons relating the D molecule. The quantum yield and the fluorescence intensity are related to each other. Hence, the higher the quantum yield the brighter the display of the emission intensity. Moreover, if the quantum yield is sensitive to the environment, it affects the fluorescence emission behavior at the same time. The quantum yield can become close to unity, when the radiationless decay rate is smaller than the radiative one but never be 1, because of the "Stokes shift". In this work the quantum yield was set to $\Phi_D = 0.184$, referring to the scientific paper of (Lingliang Long et al., 2015 [12]), which used a very similar fluorophore on the basis of the chromophore coumarin.

Generally the value of the orientation factor κ^2 can vary between 0 and 4. When the D and A molecules and its dipoles are arranged randomly

within their lifetime of excited states, its value is $2/3$[11].

6. **Solvatochromism and fluorescence quenching.**

[11], As already mentioned, energy transfer attenuation and thus a Stokes shift can be caused by various processes, such as solvent effects or complex formations.

The decrease of fluorescence intensity is called quenching and can occur by different mechanisms. One option is the collisional quenching. It takes place when the energy transfer from the excited state of the fluorophore gets prevented upon contact with some molecule in solution for example oxygen, halogens, amines or any electron-deficient molecule, conjecturing that the molecules are not chemically altered. Besides the collisional quenching, fluorophores can form non-fluorescent complexes either with other molecules or with themselves, which is referred to as static quenching, since it does not depend on molecular diffusion or collision.

[11], The solvent, as the molecular environment, plays an important role in the absorption emission spectra interpretation. There are many effects, which can affect the fluorescence as well as the quantum yields of the molecule dyes. Including the solvent polarity and viscosity, probe conformational changes, charge transfer such as protonation et al.

As a rule, the absorption spectra do not vary relatively much with change of solvent but the emission spectra can be very sensitive to environmental changes. Once the fluorophore is exited, whether to the S_1 or S_2 state, the excess vibrational energy gets lost to the solvent, due to internal conversions with in 10^{-12} s.

[11], The excited energy state can still be lowered due to stabilization by polar solvents, thus the extent of the emission shift is affected.

---

[11] (10), ch. 4 Two-Thirds or Not Two-Thirds?

Originating from the fact, that the dipole of a fluorophore is larger in the exited state than in the ground state, solvent dipoles can either re-orient or relax this exited state, by decreasing the energy gap between S_1 and S_0, resulting in emission at higher wavelengths. With increasing solvent polarity, the effect evidently increases, see figure 2.16. Bathochromism for instance, describes exactly the phenomenon of the shrinking energy gap between the molecular excited and ground state with a consequent wavelength increase.

[11], In contrast to the fluorescence lifetime, which is situated at around 10 ns, the solvent caused relaxation occurs in $(10 - 100)$ ps. However, the absorption of light measures 10^{-15} s, too short a time to be affected by the solvent and its polarity. For that reason, emission spectra of fluorophores are representative for solvent environmental effects. Absorption spectra do not show great impairment effects.

In a nutshell: the fluorophore molecule and its chromophore core react differently to various solvent environments and as a result solvatochromism is likely to be observed. An increase of the solvent polarity shifts the wavelength to higher values, called bathochromism. This effect can also be triggered by auxochromes attached to chromophore molecules. On the contrary, a hypsochromic shift often appears in connection with a removal of a conjunction or the change of the solvent polarity. The in- and decrease of the peak intensity can be attributed to the interplay and election of fluorophore in combination with the environment, in this case the solvent. Consequently, the more the fluorophores are able to interact with the UV and IR incident radiation, neglecting the quenching effects, the higher the absorbance peak will get, given in figure 2.13.

[11], In addition to the example processes characterized above, which affect the donor-acceptor RET, the most trivial type of quenching can

occur due to the optical properties of the investigated sample. Turbidity and a high optical density decrease not only the transmitted but also the fluoresced radiation intensity, responding in lacking molecular information.
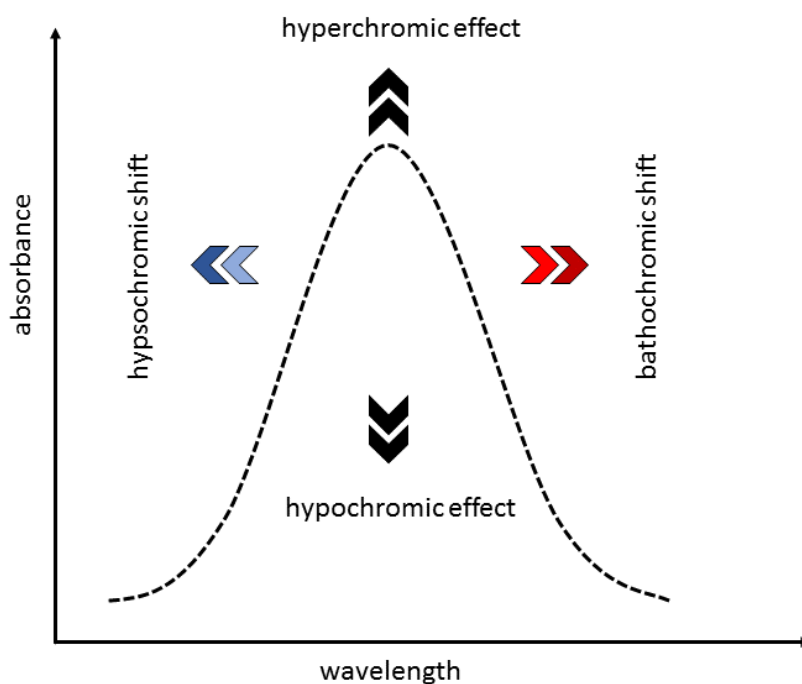
Figure 2.13: Schematics of the solvatochromism effects. Revised from [16]

Figure 2.14 illustrates exemplarily the effect of solvents on a fluorophore by means of a jablonski diagram schematic. The higher the polarity of the solvent is, the lower the excited state gets pushed down, hence the relaxing energy gap shrinks. The emission undergoes a wavelength shift to higher values (bathochromism) and in the end the fluorophore appears for example red instead of blue as at the starting point.

In Figure 2.15 legitable measured emission spectra are depicted with a dramatic impact of the increasing solvent polarity. It refers to the molecule $4 - dimethylamino - 4' - nitrostilbene$ dissolved in hexan, cyclohexane, toluene, ethyl acetat and n-butanol[12]. It shows the diversity, how various solvents can affect a single molecule.
Fluorescence intensity quenching can also occur by more trivial mechanisms such as the attenuation of incoming light by the fluorophore itself describable as an inner filtering effect or other absorbing species.

Summarizing the dependency whether the solvents themselves or the type of solvent, the result ends up in a solvatochromism, a shift of the fluorophore emission spectrum.
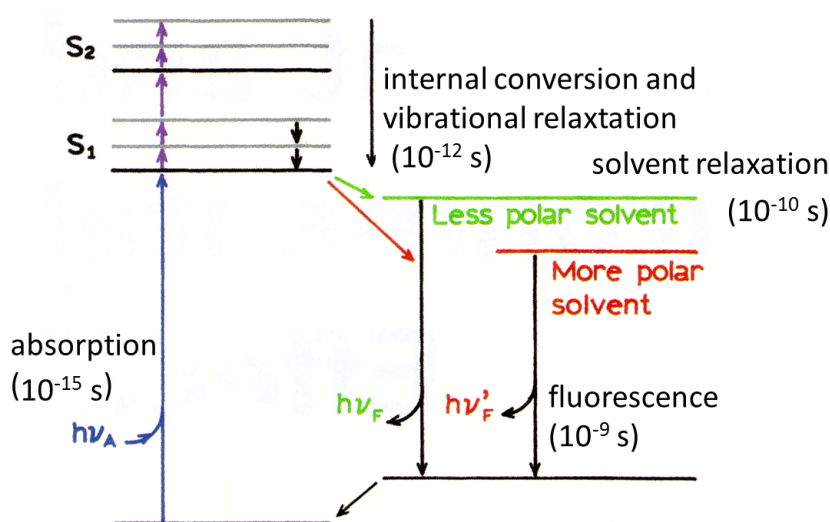
Figure 2.14: Schematics of a jablosnki diagram for a solvent affected fluorophore. Revised from [11].

_____

[12] (11), ch. 6, Solvent and Environmental Effects
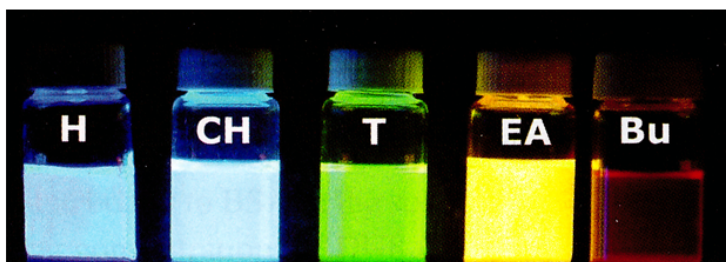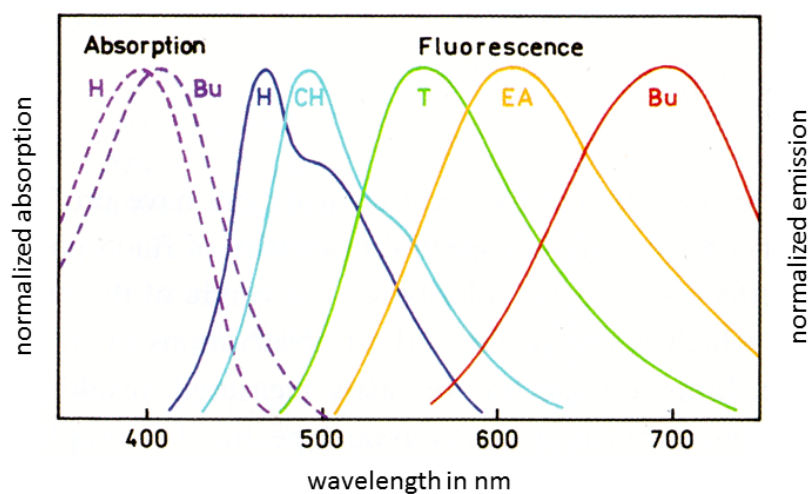
Figure 2.15: The extent of solvent polarity influence on one fluorophore concerning absorption and emission spectra. Revised from [11].

Figure 2.16 recapitulates the external environmental effects influencing the fluorophores such as solvent polarity, molecular interactions among each other or with different species, excited state reactions and molecular rearrangements, which leads to quenching, complex formation or to a RET. The term $\sum k_i$ denotes the sum of various non-radiative transitions from an excited state to the ground state aside from the quenching intensity attenuation or the RET.
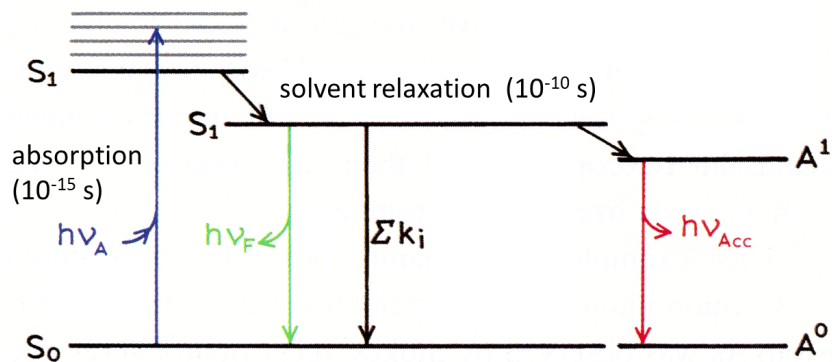
Figure 2.16: Schematics of the jablonski diagram illustrating various effects on the excited state of a fluorophore molecule. The colored arrows indicate 4 options of energy relaxation, following an absorption (blue): D fluorescence (green), radiationsless relaxations (black) and A fluorescence (red). Revised from [11]

2.3 Experimental details

This section discusses the experimental investigation path and gives a functionality overview of the measuring instruments used for this master thesis. Besides the experimental set-up, sample preparation and experimental details are described. The measuring instruments were situated in an environmental chamber with regulated amber light at standard ambient pressure, relative humidity 20 % and room temperature at around $297K$, ($Graz$, $01.06.2017 - 01.02.2018$). All measurements were carried out with a standardized quartz glass cuvette with a square base area, diameter of 1 cm, unless stated differently.

2.3.1 Instrumentation

Spectrophotometer

[17], The fundamental idea of a spectrophotometer is the investigation of light interaction with a medium. For this purpose, the light attenuation throughout a sample, the absorption measurements, were performed with a Shimadzu UV-1800 spectrophotometer. To provide a broad operation wavelength range between (190 to 1100) nm, 2 radiation sources are integrated, a deuterium and a halogen lamp, covering UV and VIS wavelengths, which were automatically switched over if necessary at around 340 nm.
Figure 2.17 depicts schematically the operating principle of a 2 beam spectrophotometer. The Shimadzu UV-1800 is a 1 chamber, 2 cuvette holder spectrometer, which allows to measure samples and references simultaneously in the same environment. This set-up allows to measure the requested molecule specimen dissolved in solution or embedded into a matrix and investigate the impact of the wavelength alternating radiation on the sample

as well as on the reference. With this insight, the environment for example a solvent, can be neglected in the course of a calculation correction, referring to 2.1.1, by taking into account, that the solvent surroundings do not strongly affect the spectroscopic properties of the fluorophores. The measuring instrument provides 3 different modes of spectrum detection: transmittance, absorption, reflection and a UVProbe software, as standard, making the control with a PC possible.
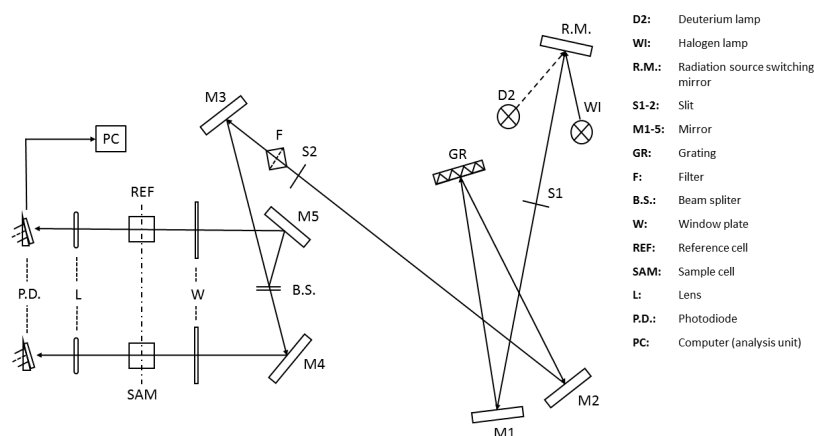
Figure 2.17: Schematics of the optical path and configuration of a 2 beam spectrophotometer. Revised from [17].

[17], In this master thesis the UV-1800 Shimadzu spectrophotometer was used as a single beam spectrometer, with the meaning, that prepared specimens and reference samples were investigated not at the same time but successively. The investigated fluorophore of interest was dissolved in different solutions and measured in a standardized quartz cuvette with diameter 1 *cm* and transmittance spectra were taken. To receive comparable recordings the instrument settings were kept always the same: the slit width - 1 *nm*, wavelength step size was - 0.5 *nm*, scanning speed set to medium with the

accumulation time of 0.2 s. Before performing measurements with the spectrometer, the apparatus was turned on, in order to let the device go through an internal checking list as well as to insure stable illumination through the 2 radiation sources. After $(20 - 30)$ min the lamps were assumed to be heated up and ready to start with the investigation measurements. To assure the reproducibility of the transmittance spectra a reference test spectrum of distilled water was recorded before starting the investigation process. This allowed also to check whether or not the cuvette was contaminated with foreign matter.

Spectrofluorophotometer

In contrast to a spectrophotometer the incident light beam, the investigated sample in a cuvette and the detector are not aligned, but arranged in a 90 degree angle.
[18], To obtain excitation and emission spectra of the utilized fluorophores dissolved in solutions, the measurements were carried out with the Shimadzu RF-5301PC with a 150 W xenon lamp, illustrated in Figure 2.18. It allows to irradiate a sample with excitation light, determined by a monochromator, and measure the fluorescence, avoiding Rayleigh-scattering. The monochromator of the incident light beam isolates a wavelength band to excite the specimen whereas the emission monochromator receives the emitted fluorescence signal and the photomultiplier tube measures the intensity. The excitation and emission sensitivity are regulated by apertures on each site. To overcome unstable light emission a light-source compensation system is regularly integrated.
The working wavelength range used in this master thesis was situated between $(200\ and\ 700)$ nm. Parameters such as scanning range, slit width and scanning speed were adapted to given circumstances as the case arises.

Xe:	Xenon Lamp
MC1:	Excitation monochromator
MC2:	Emission monochromator
B.S.:	Beam spliter
P1:	Monitor side photomultiplier tube
P2:	Fluorescence side photomultiplier tube
SAM:	Sample cell
PC:	Computer (analysis unit)
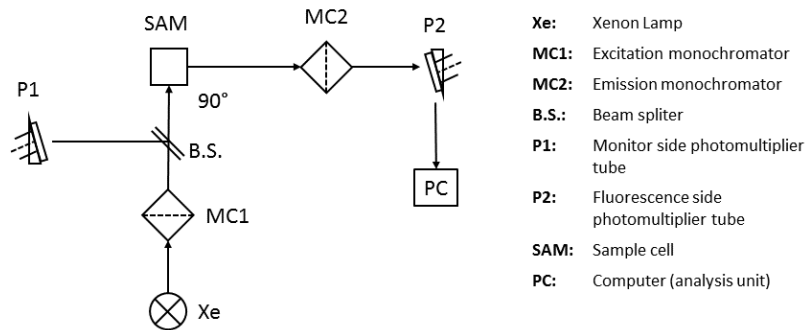
(a) Schematics of the constitution of a spectrofluorophotometer.

① Xenon lamp, 150 W
② Ellipsoidal mirror, SiO2-coated
③ Slit Assy., excitation side
④ Concave mirror
⑤ Concave grating (for excitation)
⑥ Beam splitter quartz plate
⑦ Teflon reflector plate 1
⑧ Teflon reflector plate 2
⑨ Optical attenuator
⑩ Photomultiplier for monitoring, R212-14
⑪ Condenser lens (dual-lens)
⑫ Cell
⑬ Condenser lens
⑭ Slit Assy., emission side
⑮ Concave grating (for emission)
⑯ Concave mirror
⑰ Photomultiplier for photometry, R3788-02
⑱ Focal point
⑲ Inlet slit
⑳ Outlet slit
㉑ Aperture for light quantity balancing

(b) Schematics of the optical path and configuration of the spectrofluorophotometer RF-5301PC. [18]

Figure 2.18: Schematic diagrams of a spectrofluorophotometer.

2.3.2 Used materials and sample preparation

Materials used

All of the measurements, applying the 2 investigation methods, spectrometry and fluorometry, were elaborated with 2 predefined fluorophore molecules, DCCH(**1.**) as a donor and FTSC(**2.**) as an acceptor.

These fluorophores, selected by G. Urstoeger in the course of his doctoral thesis, referring to section 1.3, were at an age of around 2 years when the project research of this master thesis began. Packed in their original amber glass cuvette, covered with additional aluminum foil, they were stored in a refrigerator in the temperature range of $(263 - 277)K$ assigned for use in a laboratory, preventing the light sensitive substances to get in contact with external radiation. Nevertheless, for the purpose of investigation and sample preparation, these cuvettes containing the fluorophores in form of a powder were opened and exposed to daylight and the surrounding air.

With the objective to broaden the knowledge base concerning the fluorophore properties in different environmental solutions, such as N,N-Dimethylformamide (DMF), water at a pH value of 9 (pH 9), further research was carried out in form of this master thesis.

Figure 2.19a and 2.19b illustrates the structural formulas of both molecules. and the following enumeration lists the materials used in this master thesis in more detail:

1. **Donor molecule, [19]**
   Name: *7-(Diethylamino) coumarin-3-carbohydrazide*
   Abbreviation: DCCH
   Empirical formula: $C_{14}H_{17}N_3O_3$

Molar mass: 275.30 $\frac{g}{mol}$
Solubility: DMF, chloroform, methanol
Fluorescence properties: $\lambda_{ex} = 450\ nm$, $\lambda_{em} = 468\ nm$ in methanol

2. **Acceptor molecule, [20]**
   Name: *Fluorescein-5-thiosemicarbazide*
   Abbreviation: FTSC
   Empirical formula: $C_{21}H_{15}N_3O_5S$
   Molar mass: 421.43 $\frac{g}{mol}$
   Solubility: DMF, H_2O
   Fluorescence properties: $\lambda_{ex} = 492\ nm$, $\lambda_{em} = 516\ nm$ in 0.1 M Tris pH 9.0

3. **standard quartz cuvette diameter** 1 *cm*

4. **capillary ringcaps "HIRSCHMANN"** 10 μl

5. **laboratory balance "Cubis Analysenwaage"** Resolution 0.1 *mg*
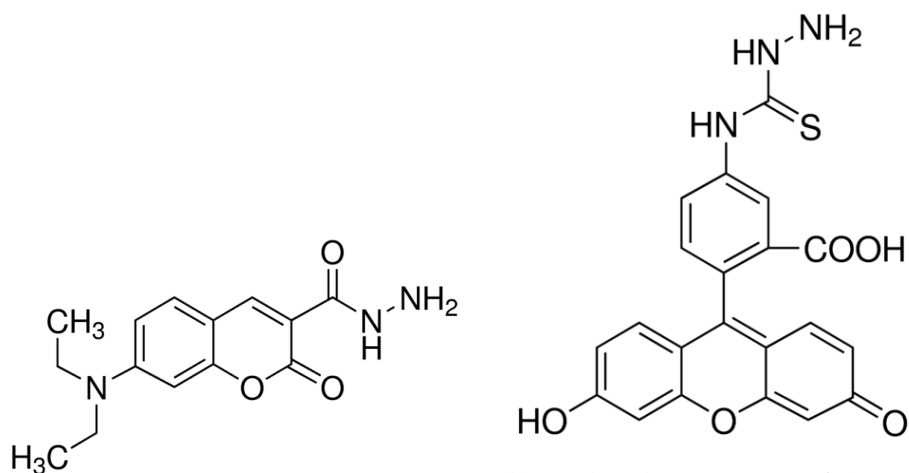
(a) Molecule structure of the donor fluorophore organized by a coumarin chromophore, a diethylamine group, and an acyl-hydrazine group with primary and secondary amines. [19]

(b) Molecule structure of the acceptor fluorophore organized by a fluorescein chromophore, with a hydroxy and a carboxylic group, primary and secondary amines with a sulfur double bond. [20]

Figure 2.19: Molecule structure of the donor and acceptor fluorophores.

The expected absorption peaks of theses 2 fluorophore molecules, according to the provided data, are situated at $\lambda_{ex} = 450\ nm$ and $\lambda_{ex} = 492\ nm$ emphasizing the aspect, that the spectroscopic properties strongly depend on the molecules environment, in this case the solutions.

Sample preparation

As part of the investigation path, various concentration series were produced following the equation

$$m = M \cdot c \cdot V \tag{2.18}$$

where m is the mass in g, M is the molar mass in $\frac{g}{mol}$, c the concentration in $\frac{mol}{l}$ and V is the volume in l. With known molar mass M, predefined concentration and volume, the required mass m of the fluorophore can be calculated for further implements.

These preprocessed concentration probes of the fluorophore were diluted by using

$$C_1 \cdot V_1 = C_2 \cdot V_{tot} \quad with \quad V_{tot} = (V_1 + V_S) \tag{2.19}$$

where C_1 is the starting concentration in $\frac{mol}{l}$ of the given fluorophore dissolved in solution with the volume V_1 in ml. According to that, the sum $V_1 + V_S$ defines the volume of the outcome solution with the concentration C_2 and the volume of the added solvent V_S.

However, the volume contraction, id est, the decrease of the total volume, was not taken into account, since the amount of fluorophore substance was assumed to be small enough. This effect occurs, for example, by mixing water and alcohol together: 48 ml water plus 52 ml alcohol do not result into a total volume of 100 ml, but less.

In order to determine the amount of RET between the 2 fluorophores as a result of fluorescence, both, FTSC and DCCH were mixed in different ratios. To calculate the volume of the requested concentration ratios, the following steps were deduced from equation 2.19 while taking the assumption, that the fluorophores dilute mutually ($C_1 V_1 = C_1'(V_1 + V_2)$ and $C_2 V_2 = C_2'(V_2 + V_1)$). Combination of the equation 2.19 and the 2 relations lead to

$$C_1 \cdot V_1 = C_1' \cdot \frac{C_2 V_2}{C_2'} \rightarrow \frac{C_1 V_1}{C_2 V_2} = \frac{C_1'}{C_2'} = R \tag{2.20}$$

To obtain a reliable investigation result with the standardized cuvette according to the set-up and the incident light beam alignment in the mounting brackets of the spectrophotometer as well as of the spectrofluorophotometer, the content of the cuvette, was limited to around 4 ml. (Maximum filling of the used cuvette was measured to be 4 ml). Thus the volume could be chosen variable $V_1 + V_2 = X$ ml in the range of $(2 - 4)$ ml as a secondary condition. This results in

$$\frac{C_1 V_1}{C_2(2 - V_1)} = R \rightarrow V_1 = \frac{\cancel{R} \cdot X C_2}{\cancel{R}(\frac{1}{R}C_1 + C_2)} = \frac{X C_2}{\frac{1}{R}C_1 + C_2} \tag{2.21}$$

$$with \quad R \in [\ldots \frac{5}{1}, \frac{2}{1}, \frac{1}{1}, \frac{1}{2}, \frac{1}{5}, \ldots]^{13}$$

R, in this case represents the desired concentration ratio between donor and acceptor molecules in solution. Knowing the starting conditions C_1 and C_2, concentration series of donor-acceptor mixtures can be produced. V_2 can be derived from V_1.

The same results can be achieved by applying

$$C_1' = \frac{C_1 V_1}{V_1 + V_2} \tag{2.22}$$

C_1' expresses the concentration of one fluorophore species after dilution by the other species.

The following 2 steps illustrate the theoretical manufacturing process starting from weighting the chromophore mass up to diluting the initiation solution to a desired outcome. With regard to the solutions of dissolved chromophores, the change of the partial molar volume (the change in volume per mole in a mixture of at least 2 different substances) was neglected.

---

[13]These concentration ratios were used, but shall not be obliged.

It is an exemplary calculation path and serves for demonstration.

1. **Weighting required chromophore mass**
   First, the fluorophore substances, given as fine powders, were weighted out with a laboratory balance and preserved in an amber glass cuvette to protect the content from light irradiation.
   Assuming an outcome volume $V = 5\ ml$ of dissolved FTSC in water and a concentration $c = 1\ \frac{mmol}{l}$ the mass m in equation 2.18 calculates to $m = 2.11\ mg$ with the given molar mass of FTSC $M = 421.43\ \frac{g}{mol}$.
   In case the required mass was measured with slight deviations, the concentration was recalculated to the volume to obtain the correct value.

2. **Diluting process**
   Starting from the concentration of the chromophore dissolved in solution, $C_1 = 1\ \frac{mmol}{l}$, referring to equation 2.19, with the required concentration $C_2 = 0.5\ \frac{mmol}{l}$ and the volume $V_{tot} = 2\ ml$ both of the volumes, V_1 and V_2 calculate to $1\ ml$. In consequence the concentration ratio of solvent and solute yields 1 : 1.

3. **Concentration variations**
   When mixing 2 species at different concentrations, each of them gets for itself diluted by the counter part. The following examples show, how the single concentrations were calculated. Once the fluorophore solutions are prepared separately, D-A solution mixtures can be produced in different concentration ratios and volumes according to the starting values.

   - Referring to equation 2.21
     Starting parameters: $R = \frac{C_1'}{C_2'} = \frac{2}{1}$, $C_1 = C_2 = 1\ \frac{mmol}{l}$, $X = 3\ ml$

$$V_1 = \frac{XC_2}{\frac{1}{R}C_1 + C_2} = \frac{3 \cdot 1}{\frac{1}{2} \cdot 1 + 1} = 2 \tag{2.23}$$

$V_1 = 2\ ml$ and $V_2 = 1\ ml$

$$C_1' = \frac{C_1 V_1}{X} = \frac{2}{3} \tag{2.24}$$

$C_1' = \frac{2}{3}\ \frac{mmol}{l}$ and $C_2' = \frac{1}{3}\ \frac{mmol}{l}$

- Referring to equation 2.22
  Starting parameters: $R = \frac{V_1}{V_2} = \frac{2}{1}$, $C_1 = C_2 = 1\ \frac{mmol}{l}$

$$C_1' = \frac{C_1 2V_2}{2V_2 + V_2} = \frac{2}{3} \tag{2.25}$$

$$C_2' = \frac{C_2 V_2}{V_2 + V_1} = \frac{1}{3} \tag{2.26}$$

$V_1 = 2\ ml$ and $V_2 = 1\ ml$
$C_1' = \frac{2}{3}\ \frac{mmol}{l}$ and $C_2' = \frac{1}{3}\ \frac{mmol}{l}$

With the formulation above, the concentrations C_i' after the D-A mixture production could be calculated. This information will be needed later on in section 4.2.1, to determine the FRET efficiency.

Preparations beforehand

Distilled water at pH 9 was produced based on an alkaline buffer solution with di-Sodium tetraborate decahydrate also known as BORAX [14].

---

[14][21], BORAX a synonym for di-Sodium tetraborate decahydrate was used to prepare an aqueous alkaline solution.

A buffer is an aqueous solution acidic or alkaline, which does not strongly change its pH value by adding acids or bases. As a consequence, buffer solutions are used to keep the pH nearly constant in chemical applications. Using equation 2.18 the mass m, id est the grammage of BORAX, can be calculated to $m \approx 0.95$ g assuming a concentration c of 5 $\frac{mmol}{l}$ and a volume $V = 0.5$ l. The molar mass M of BORAX is given as 381.37 $\frac{g}{mol}$.

3 Experimental implementation

This section describes the experimental part conducted by spectrophotometry and spectrofluorophotometry and depicts achieved results of taken measurements with additional explanations of important characteristics and features concerning the change of development.

Due to the enormous data set, it was not expedient to list all gathered spectra data carried out, but present and demonstrate descriptive results exemplarily. In the course of the investigation process various different concentration solutions with D and A fluorophores were prepared. The concentration values range from a hundredth of micromole per liter up to the saturation limit at $c_{DS} \approx 0.14 \, \frac{mmol}{l}$ and $c_{AS} \approx 0.3 \, \frac{mmol}{l}$ of D and A, respectively, dissolved in pH 9. The process of dissolution was performed at standard room temperature conditions, referring to section 2.3.

3.1 Process chain

The following figures 3.1, 3.2 present the whole investigation path, applied methods and procedures of data collection in a block diagram with 2 branches, processed from left to right. Starting from the fabrication of the fluorophore solutions up to the recording of the required spectra via spectro- photometry and fluorophotometry upto the calculations of the

defined figures of merit, the Förster distance and the FRET efficiency.

To assure the reproducibility of the spectrum measurements before any experiment, the quartz cuvette was cleaned at first with propan-2-ol (Isopropanol) and afterwards with distilled water, repeatedly, so that the removal of possible remnants was ensured. Further on, both, the spectrophotometer as well as the fluorophotometer were switched on for at least 20 *min* to heat up the radiation sources to achieve stable illumination conditions. The light beam alignments and investigation chamber cleanliness was verified and to ascertain a proper mode of system operation a reference record of pH 9 was taken as the very first spectrum, using the spectrophotometer. As a whole, the sample preparations and spectra recordings were realized as a standardized process.

The first block segment in the schematic (top left branch) illustrates the chromophore molecules, donor and acceptor, dissolved in 3 different solutions. Different concentrations were produced and transmittance raw data spectra were taken with the spectrophotometer, saved as relative intensity over wavelength. According to section 2.1.1, first, the corrected transmittance $\frac{I}{I_0}$, the absorbance or optical density and lastly the extinction coefficient spectrum were calculated. The absorbance, however, was background corrected with a linear offset to get rid of spectroscopic irregularities such as reflection effects, which in consequence influences the subsequent calculations. As can be seen in Figure 3.1 (bottom left branch), the focus was set on determining the acceptor extinction coefficient, one of the essential parameters to compute the overlap integral, depicted in the following Figure 3.2.
Second, the donor emission spectrum was recorded with the spectrofluorophotometer and area normalized to unity. On the following pages it will turn out, that the preferential solvent was chosen, hence the fluorophore investigation was dominantly performed with pH 9, shown in the right

branch, Figure 3.1. With these 2 data inputs and taking all additional inputs mentioned in section 2.2 into consideration (Φ_D, κ^2, n), the overlap integral J and further the Förster distance R_0 were determined using equation 2.10 and 2.17, respectively.

In the end, the FRET efficiency was calculated, defined through the donor quenching and acceptor sensitization. This information provides details of the performance between the two fluorophore molecules in dependence of their environment and proves the possibility of a RET.
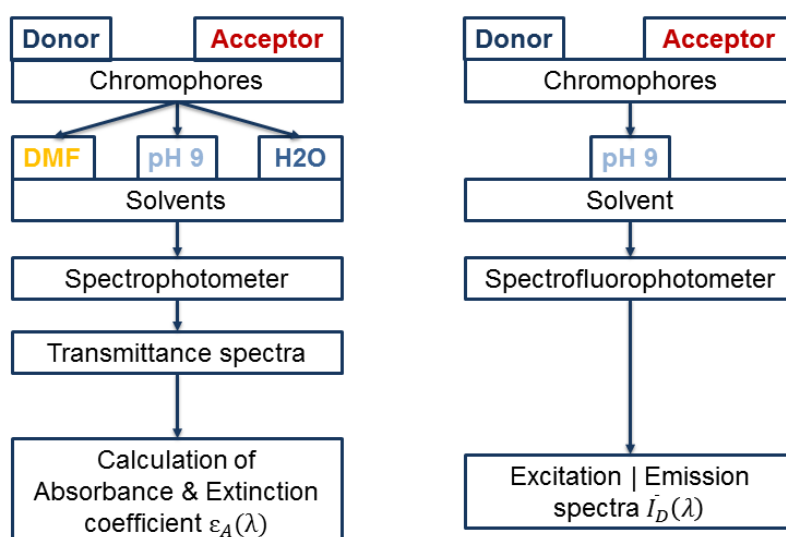
Figure 3.1: Schematics of investigation path and methods depicted in a 2 branched block diagram, processed from left to right.
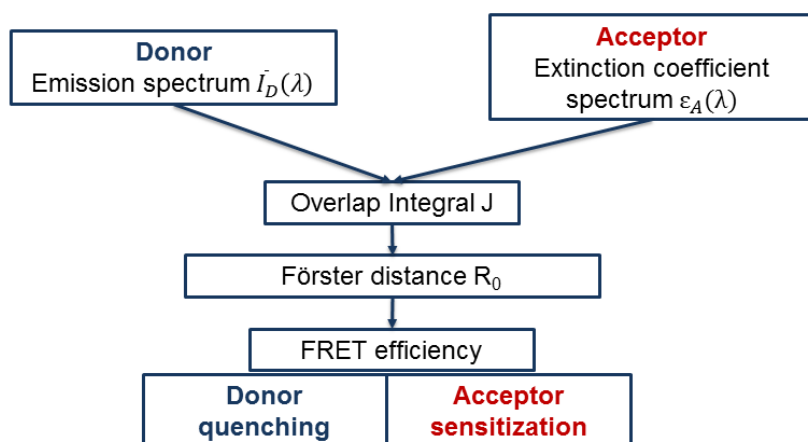
Figure 3.2: Schematics of the overlap computation between acceptor extinction coefficient and donor emission spectrum.

3.2 Spectrophotometer

Spectrophotometry was used to collect transmission spectra data and to cal-
culate subsequently the absorbance and extinction coefficient of the acceptor
molecule dissolved in a predefined solvent (referring to the left branch 3.1).
Figure 3.3 shows, firstly, the transmittance spreading of empty quartz cu-
vettes and secondly, the transmittance raw data spectrum of the spectropho-
tometer Shimadzu UV1800. The raw data transmittance spectrum of the
standardized cuvettes depicts a stable, absorption-free behavior in the whole
measuring range of the Shimadzu device with a relative intensity value
lower than 1%. Secondly, the figure illustrates the transmittance perfor-
mance of the light radiation channeled through the wavelengths from NIR
upto UV. At around 340 nm an absorption peak is clearly evident, which is
caused by merging the deuterium and halogen radiation sources. Due to a
switching delay this small intensity drop occurs.
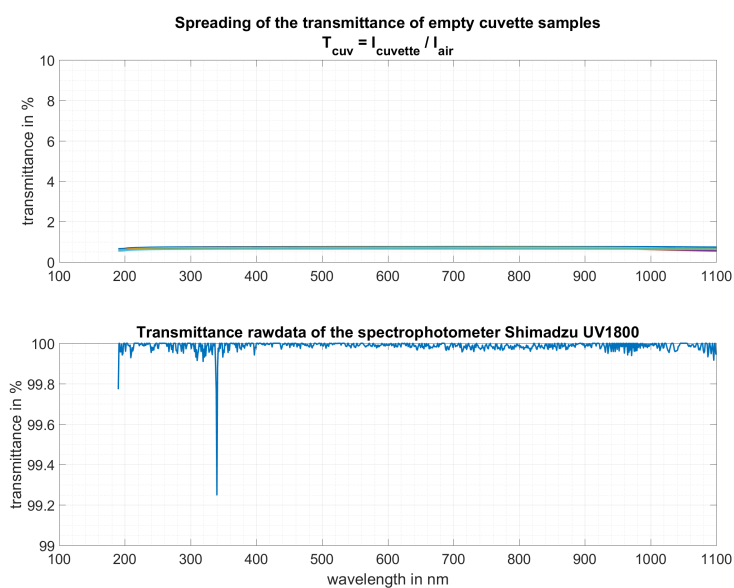
Figure 3.3: Transmittance spectrum of spectra of cuvettes without content and empty chamber of spectrophotometer at room conditions.

The following 3 curves of used pure solvents, depicted in figure 3.4, were used to investigate the 2 fluorophores, DCCH and FTSC. All of them do not show any absorption behavior from $(300 - 700)$ *nm* in the raw data transmittance diagram. Therefore, the solvents have no indication to affect the fluorophores a priori.
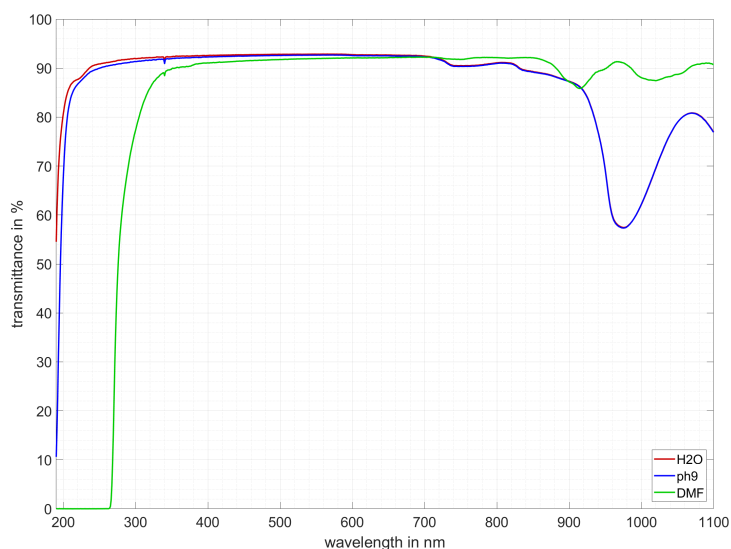
Figure 3.4: Raw data transmittance spectra of pure solvents used for investigation.

The designated, first investigation step was the characterization of the fluorophore molecules in DMF solvent with spectrophotometry. Figure 3.5 shows 5 transmittance raw data spectra, relative intensity over wavelength: the green line depicts DMF as pure solvent and the 4 remaining spectra show FTSC dissolved in DMF with increasing concentration $(0.01, 0.1, 1, 3)$ $\frac{mmol}{l}$. At low concentration values, $(0.01, 0.1)$ $\frac{mmol}{l}$, the absorption curve does not exhibit measurable absorption effects. Whereas 1 $\frac{mmol}{l}$ shows ripples and 3 $\frac{mmol}{l}$ starts to form a valley due to absorption at around $(450 - 500)$ nm. Also visible is the systematic transmission behavior between increasing FTSC concentration in DMF and relocation of the absorption edge to higher wavelengths, defined as a bathochromic shift.
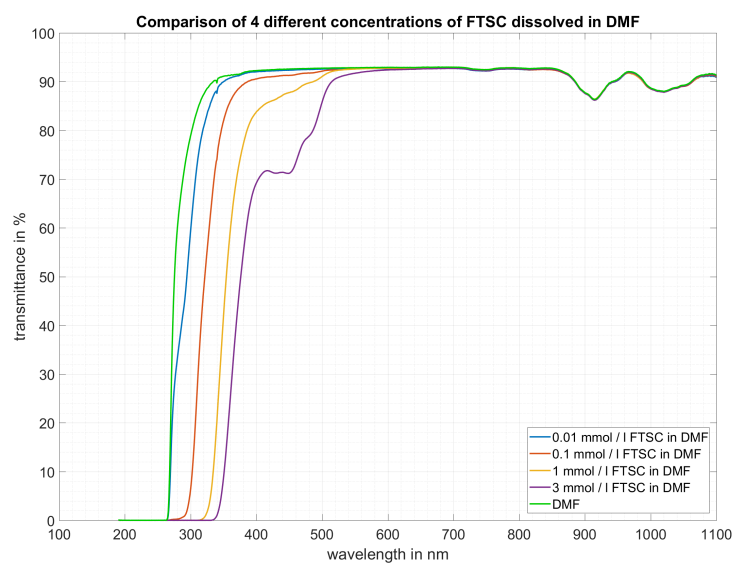
Figure 3.5: 4 different raw data transmittance spectra of dissolved FTSC molecule in DMF with increasing concentration $(0.01, 0.1, 1, 3)\ \frac{mmol}{l}$ and the pure solvent DMF depicted in green.

At this point it needs to be emphasized, that with the measurement results shown in Figure 3.5, the functionality of FTSC dissolved in DMF did not reach a profound verification, although the concentration of 3 $\frac{mmol}{l}$ shows a clear absorption behavior. Even though the measurements with the solvent DMF seemed to be a promising approach, it was considered, to change the solvent into distilled water at pH 9 due to 2 general reasons:

1. **Correlation of solvent behavior and bonding mechanisms**
   Dimethylformamide (DMF), is an organic, polar solvent used in many applications such as reagent, it is a common catalyst, serves as solvent itself or provides the basis of different dissolvers (cosolvent). It was predicted to have an unwanted influence on the fluorophore molecules themselves, on the prospective produced cellulose fibers and a nameless impact on their bonding mechanisms. Moreover, fibers, which are made up by cellulose, connected via hydrogen bonds, could be affected by a preceding dyeing process with DMF. Since the reactivity of cellulose systems is mainly determined by the interaction between external anions and the hydroxyl protons, remnants of DMF on the fluorophores or the fibers could compromise or falsify the results of targeted investigations. Apart from the fact, that DMF is not part of the paper-making process, but water.

2. **FTSC in pH 9**
   However, water and its modifications in pH values constitutes a more natural material to cellulose fibers and convenient solvent considering the fiber-fiber interactions, which was resolved to be the investigation basis in the course of this research project. Furthermore, the doctoral thesis, from which this work was branched off, added an inducement by conducted data of previous fiber-fiber interaction measurements in water at pH 9.
   DMF was thought to play a significant role in influencing the hydrogen

bonds, the capillary bridges and swelling behavior of cellulose fibers.

Figure 3.6 illustrates donor and acceptor transmittance raw data, both of them dissolved in DMF (red) as well as in pH 9 (blue). 0.05 $\frac{mmol}{l}$ donor does not seem to be affected by the change of solvent ingredient regarding the absorption peak depths, shown in figure 3.6a. The absorption peaks are shifted and represent an option of solvatochromism, but not essential for further investigation steps. Whereas the acceptor with the same concentration and its 2 solution states dissolved in DMF and pH 9 differ strongly from each other, figure 3.6b. In the range of 420 nm the acceptor in DMF forms a local minimum with 90% counts according to the relative transmittance intensity (see figure 3.6b). However, in comparison to that, dissolved in pH 9, it shows a very steep absorption peak with $\lambda_{max} \approx 490$ nm and the spectrophotometers detector is still in saturation at this concentration (see figure 3.6a).

While the absorption position of the donor molecule differs from the given data, fluorescein, the chromophore component of the acceptor molecule, see section 2.3.2 bullet **2.**, shows suitable absorption behaviors at 490 nm.

Referring to a similar fluorophore molecule called fluorescein isothiocyanate (FITC)[1], FTSC matches the optical absorption properties. On the contrary, the behavior of the donor molecule, DCCH, is not comparable to the data prescribed in section 2.3.2 bullet **1.**, because of different solvent used. However, the magnitude of the absorption wavelength range is given.

The absorption minima of both molecules monitor the fluorophore specific absorption properties, depending on the chromophore basis and the functional groups attached. Furthermore, the dependency on the utilized solvent and its fluorophores can be already observed:

---

[1] (11), ch. 3 Fluorophores

different solvent lead to different absorption behaviors of the chromophore core molecules.

[22], Besides the molecular specific absorption peaks around $(400 - 500)$ nm, there is another peak displayed at $(970 - 980)$ nm. This peak belongs to the combination bands, including the symmetric and asymmetric water molecule stretching modes at 1450 nm and 970 nm. In other words, the band at 970 nm is referred to the 2_{nd} overtone of the OH stretches, which lies in the NIR region of the electromagnetic spectrum, where almost exclusively can be found overtone bands.
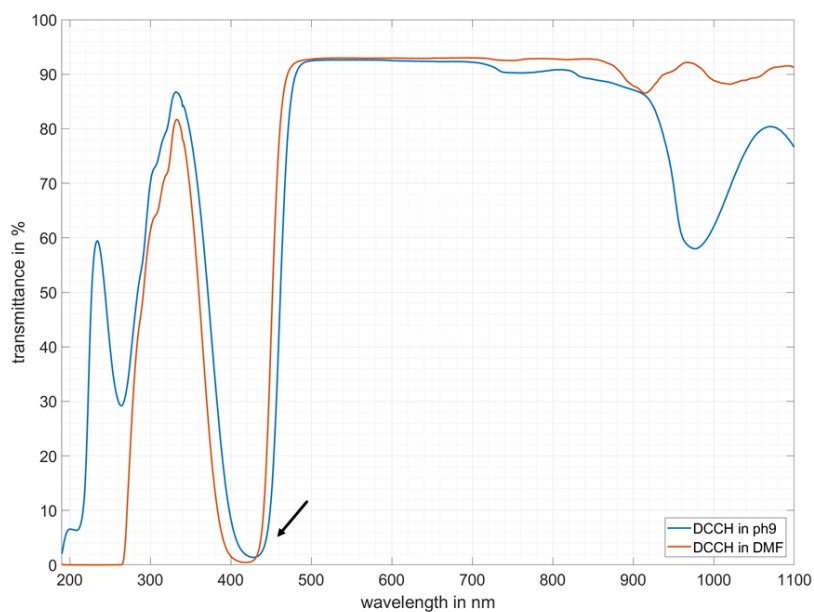
(a) Transmittance raw data of 0.05 $\frac{mmol}{l}$ DCCH dissolved in DMF (red) and pH 9 (blue).
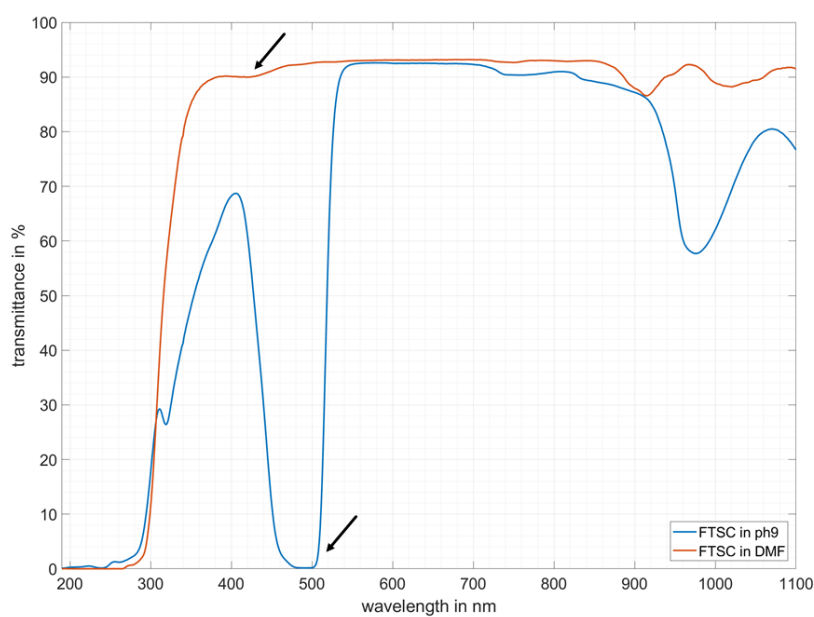
(b) Transmittance raw data 0.05 $\frac{mmol}{l}$ FTSC dissolved in DMF (red) and pH 9 (blue).

Figure 3.6: Transmittance raw data spectra of donor and acceptor, both dissolved in DMF and pH 9.

Although the performance of FTSC in DMF is known, it also shows profound properties suitable for fluorescence in pH 9, see section 2.3.2. For these 2 reasons pH 9 was constituted to be the amendment of the investigation process and chosen as preferential solvent and environment of the fluorophores to be studied with.

In addition to the choice of preferred solvent to investigate the fluorophores with and in accordance with the signal saturation of the detector, the solvents concentration was apparent to be lowered in order to achieve informative transmission results.

Figure 3.7 depicts a concentration series of FTSC dissolved in pH 9. As expected, the absorption minima peak positions do not change in the course of diluting and are situated at around $(480-500)$ nm but the concentration of 0.05 $\frac{mmol}{l}$ (red curve) can not be optically dissolved by this set-up. $\frac{1}{5}$ of the concentration yields providing 10% transmittance. The lowest concentration in this series, 0.001 $\frac{mmol}{l}$, shows nearly 80% transmittance in the same wavelength range.
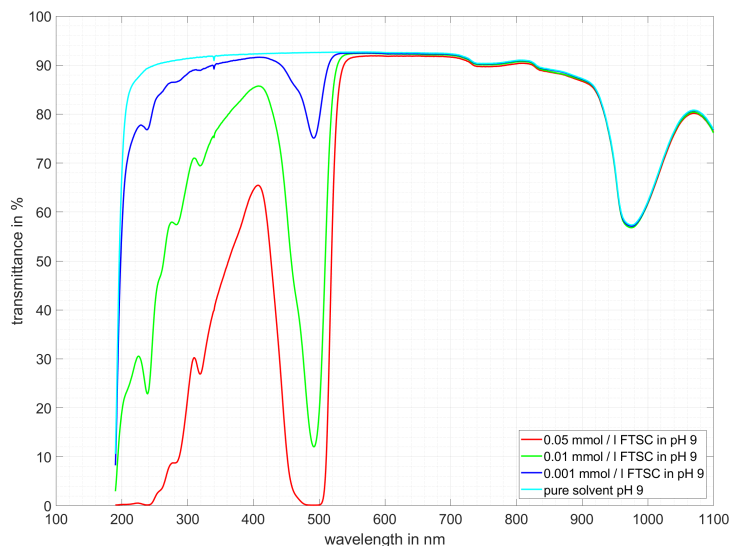
Figure 3.7: Raw data transmittance spectra series of FTSC dissolved in pH 9.

Figure 3.8, divided into the parts *a)* and *b)*, shows the light path through the quartz glass cuvette (C) mounted in the cuvette holder (CH). The light, form the radiation source (RS), adjusted perpendicular onto the surface, interacts with the probe content and the outcome is recorded by a detector located precisely behind the cuvette - light source, cuvette and detector are arranged in 90 degrees angle along one plane. Thus the operator and spectator observes the set-up in a profile view.

As this figure implies, the fluorophores are not dark quenchers, but luminescent molecules on the example of: 2 *ml* 0.05 $\frac{mmol}{l}$ A dissolved in pH 9[2]. In part *a)* 2 features can be seen: First, the incident light beam from the radiation source has a different wavelength compared to the fluorescence coming from the interaction volume in the cuvette. The former one can be

---

[2]Figure 3.8 shows exemplary 2 video cut outs of the measurement 0.05 $\frac{mmol}{l}$ FTSC in pH 9 depicted in figure 3.7. The footage was taken from an open side window recorded with a Samsung Galaxy S6 Edge.

seen clearly as a reflectance on the chamber wall, on the left, tinned in blue. To the right, the leaving radiation appears in the same color, but fainted and blurred. Second, the incident light beam goes straight through the sample and the interaction volume, over the entire width of the cuvette, shines greenish and bright. In contrast to part *a*), the light beam in part *b*) does not penetrate the whole width of the cuvette content. Instead of a straight band, the resulting fluorescence area forms a cone.

Referring to the spectral data in figure 3.7, the exemplary fluorescence data from part *a*) could originate from an excitation wavelength in the range of $(400 - 450)$ *nm*, where the transmittance values count up to 60% relative intensity. Comparing the escaping light on the right side of picture *b*), to the electromagnetic spectrum, the resulting color yields into light blue, cyan or turquoise, which will correspond to a wavelength of 490 *nm* or a little higher.

The most obvious characteristic is the greenish fluorescence, which indicates the maximum emission wavelength λ_{em} situated around 500 *nm*, taking the stoke shift effect into account.

In the following pages, these conclusions, based on vague assumptions, will be reinforced and confirmed.
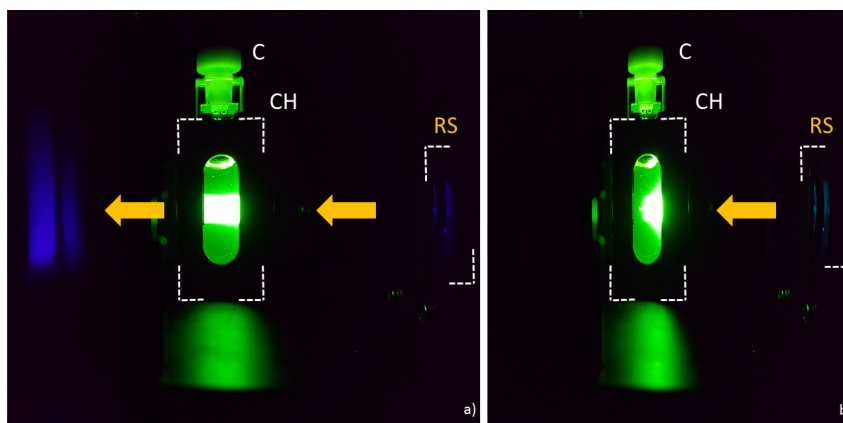
Figure 3.8: Light path through a standard quartz glass cuvette filled with 2 *ml* 0.05 $\frac{mmol}{l}$ FTSC dissolved in pH 9.

3.3 Spectrofluorophotometer

The spectrofluorophotometry was primarily used to get information about the donor emission and acceptor excitation spectrum overlap. Furthermore, it enables to monitor the variance of the donor and acceptor emission spectrum as it is expected the former to decrease and the latter to increase over the course of RET.

Figure 3.9 serves as a conceptual crossover between the 2 measuring types, the spectro- fluorophotometry and photometry. For the purpose of illustration all spectra were normalized to unity in this figure.

In the first row the excitation and emission spectra of the donor molecule are depicted. In return, the acceptor is shown at the second row. The spectra measurement series of 3 different concentrations $(0.05, 0.01, 0.001) \frac{mmol}{l}$ tinted in red, green, blue were carried out with different fluorometry settings to provide an optimal fluorescence performance of the fluorophore molecules dissolved in pH 9. The D excitation spectrum of $0.05\frac{mmol}{l}$ was recorded at a wavelength of 485 nm and the emission spectrum was carried out at an excitation wavelength of 375 nm.

The excitation spectra of both fluorophores at $0.05 \frac{mmol}{l}$ evince a vast bump, 2 peaks with a valley, between $(400 \; and \; 500) \; nm$. These curves result in a verification of the measurements done with spectrophotometry, referring to figure 3.6. The concentrations of the 2 fluorophores dissolved in pH 9 were too high to be investigated properly using this set-up.

Another feature the presentation method allows to see, is the bathochromic shift with increasing concentrations at the A emission spectra.
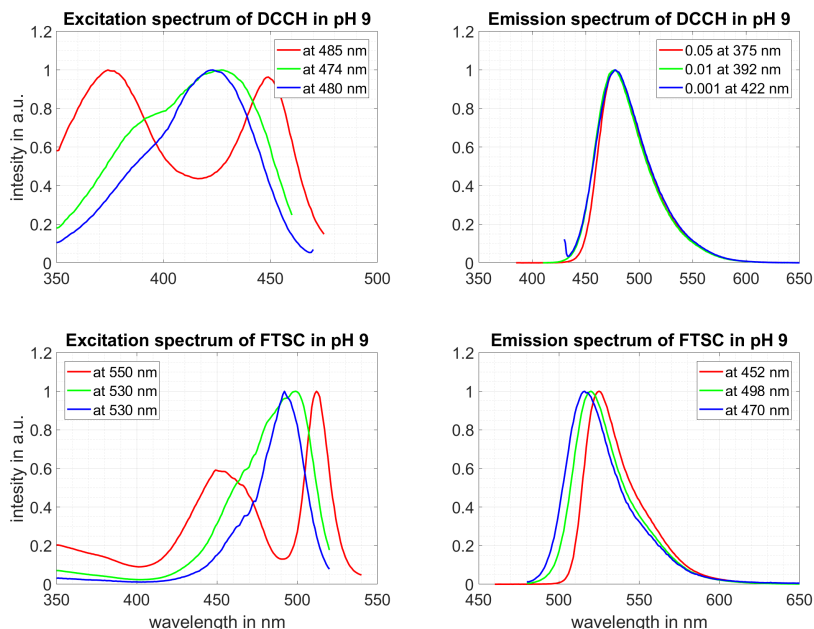
Figure 3.9: Exciation and emission spectra of DCCH and FTSC at 3 different concentrations. $(0.05, 0.01, 0.001) \frac{mmol}{l}$ tinted in red, green, blue were carried out with different fluorometry settings.

The following graphic, figure 3.10, shows the excitation and emission spectra of both fluorophores, diluted to 0.001 $\frac{mmol}{l}$ in pH 9. Furthermore, it depicts the wavelength positions, at which maximum absorption (excitation) and fluorescence (emission) takes place: $\lambda_{ex}^D = 423$ *nm* and λ_{em}^D lies at 478 *nm*. $\lambda_{ex}^A = 492$ *nm* of the acceptor and it fluoresces at $\lambda_{em}^A = 516$ *nm*.

Due to the fact, that the fluorophores respond differently to the incident light, the spectra curves were normalized to unity, in order to illustrate collectively the shape and position of the peaks. The overlap of the D (blue) emission and the A (red) excitation spectrum is illustrated with continuous lines $(-)$, whereas the D excitation as well as the A emission spectra are given with dashed curves $(--)$.

But caution has to be taken, when studying the spectra. In this condition

the figure shows the shape of the excitation and emission fluorescence as well as their maxima. These spectra illustrate a qualitative not a quantitative comparison. Thus, the amount of spectral overlap can not be weighted correctly in this figure, but the position of their maxima and the relative data values according to the normalization.

On the basis of spectral behavior, the majority of the recorded fluorescence emission spectra were done at the wavelength $\lambda = 400 \ nm$, highlighted with a marking. It was chosen to optimize the excitation of the D composition and at the same time minimize this effect on the A side. As can be seen, the outlets of the A at 400 nm are nearly 0 but the D counts around 0.8 of its relative intensity.

$\lambda_{ex} = 400 \ nm$
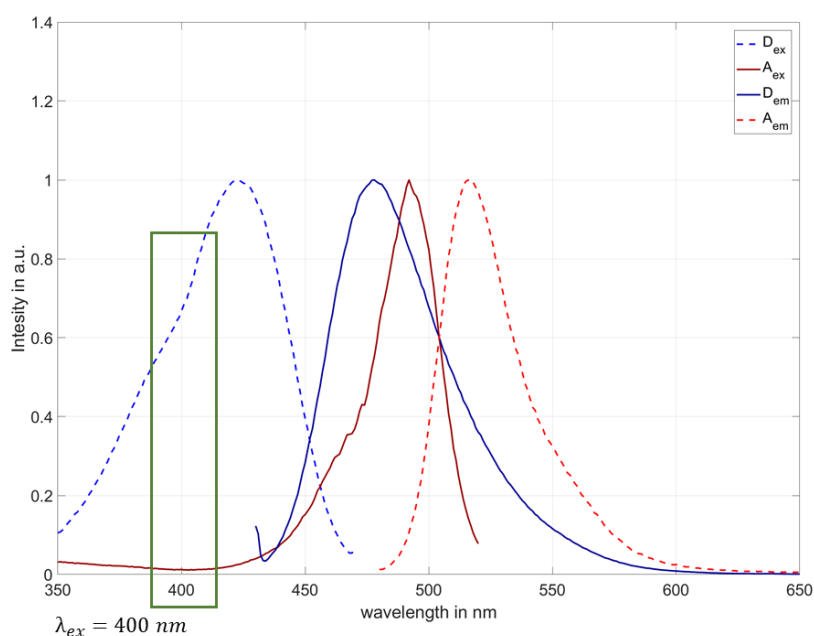
Figure 3.10: Excitation and emission spectra comparison of DCCH and FTSC at normalized conditions. On the basis of spectral behavior, the excitation wavelength chosen to be at $\lambda = 400 \ nm$.

4 Data analysis and results

This part of the work deals with data processing of records carried out with spectrophotometry and spectrofluorophotometry. The collected spectra were edited in order to calculate the predetermined figures of merit, the Förster distance and the FRET efficiency.

The analyzed results of activities in research are presented throughout 2 examples of different concentration ratio series between the D-A compound solution. First, the investigation process to calculate the Förster distance is discussed, and secondly, the FRET efficiency, defined as a figure of merit, with the goal to present the possibility of a successful RET by observing fluorescence.

4.1 Förster distance

For the purpose of calculating the Förster distance R_0, the D emission as well as the A absorbance spectra were computationally preprocessed to receive the required molecule specific spectra in a predefined wavelength range. To receive an overview of the D-A interplay, measurement series of fluorophore ratios were made, to investigate the fluorescence output sensitivity in dependence of the relative concentrations, with the objective to observe A fluorescence following RET.

Figure 4.1 illustrates an overview on the determination of the Förster distance with the required work packages. On the one hand the D emission spectrum, recorded with fluorometry was area normalized, on the other hand the absorbance peak, resulting from spectrophotometry, was first background corrected and second the extinction coefficient spectrum was determined.

On the basis of the corrected D emission and A extinction coefficient spectra, the Overlap Integral J was calculated. With the given characteristic parameters, the fluorescence quantum yield of the donor Φ_D, the dipole-dipole orientation factor κ^2 and the refractive index of the solutions n to the power of 4, the Förster distance R_0 was determined.
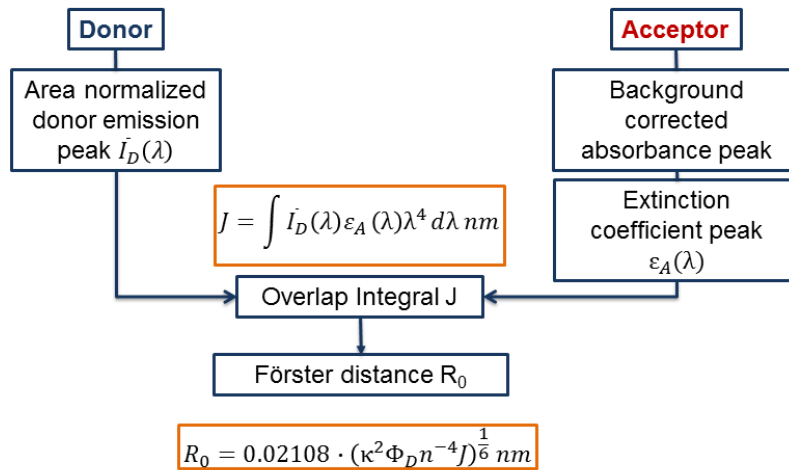
Figure 4.1: Block diagram illustrating the realization of the Förster distance calculation.

Linear baseline correction

The background correction based on a linear baseline offset, was conducted to form the absorbance peaks and subsequently assure well defined spectra peak realizations, schematically shown in figure 4.2. In order to control the

impact of the base line correction and the location of the minima with the help of an algorithm, 2 intervals were introduced, marked with the dashed lines.

The interval locations were defined at the edges of the absorbance signal peak, assuming that these peaks would not change their shape dramatically. Subsequently the intervals were narrowed, always checking for the minimum in each of the intervals, respectively. Since the initial data (green) was not smoothened or edited in any ways, this method was applied, to restrict the selection of supporter points and localize the optimal points (red crosses) of the peak range, resulting in a tangent (dashed red line), being aware of the measurement uncertainties of the instrument.
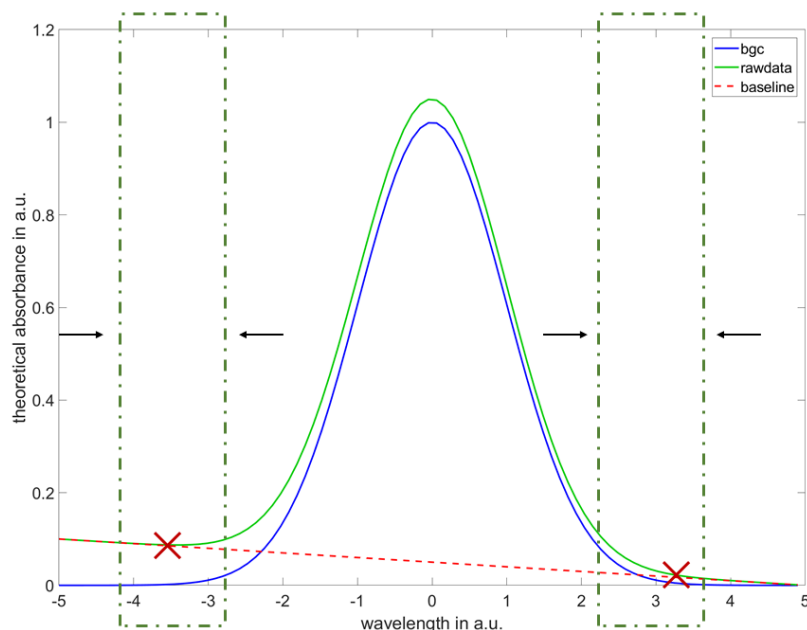
Figure 4.2: Theoretical illustration of the background correction on the basis of a linear baseline.

The absorbance, figure 4.3, referring to the transmittance measurement data of 0.05 $\frac{mmol}{l}$ D and A dissolved in DMF as well as in pH 9 depicted

above, was calculated according equation 2.7. The curves with dashed lines describe the fluorophores dissolved in pH 9 and the continuous ones, show the absorption peaks corresponding to the solution in DMF. These 2 figures once again demonstrate the optical behavior of both fluorophores in dependence of concentration. In comparison to the D molecule, which does not seem to be affected by the solvent change, except of a small bathochromic shift, the optical behavior of A molecule is clearly influenced by the solvent within this concentration configuration.

At this point the aqueous solvent at pH 9 was prioritized for the investigation process.
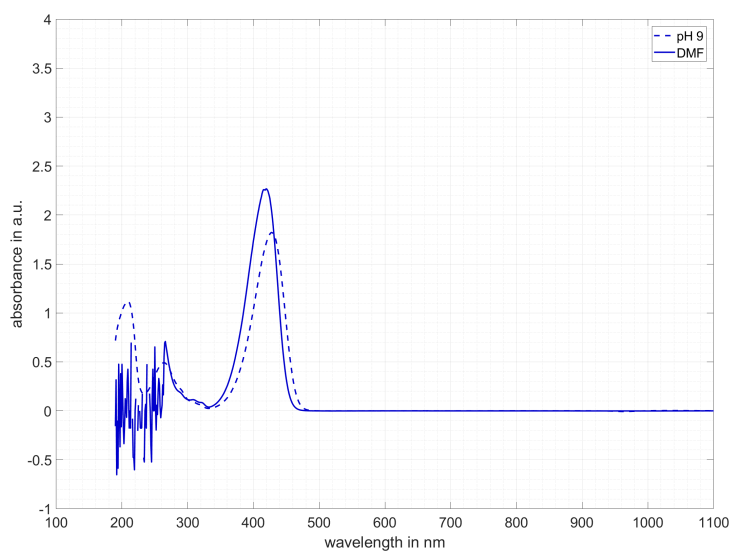
(a) Absorbance spectra of $0.05 \frac{mmol}{l}$ DCCH dissolved in DMF $(-)$ and pH 9 $(--)$.
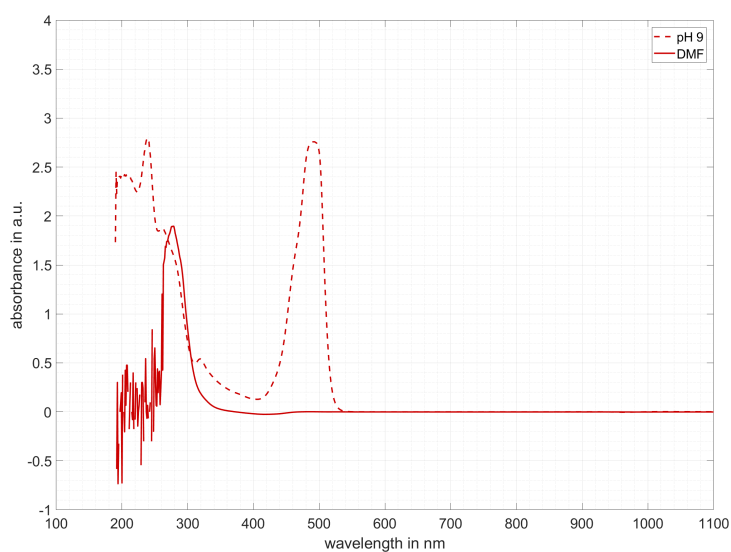
(b) Absorbance spectra of $0.05 \frac{mmol}{l}$ FTSC dissolved in DMF $(-)$ and pH 9 $(--)$.

Figure 4.3: Absorbance spectra of donor and acceptor, both dissolved in DMF and pH 9.

The extinction coefficient in dependence of the wavelength $\epsilon(\lambda)$ was determined via equation 2.8 in the range of $(190\ to\ 1100)\ nm$. These curves give information about the absorption behavior of the single fluorophores independent of their concentrations. Exceptions occur if, either the concentration of the fluorophore in the solvent is too low or oversaturated, to be optically dissolved by the detector. The latter phenomenon is shown in figure 4.4. The concentrations $(0.01\ and\ 0.001)\ \frac{mmol}{l}$ are relatively small not to be in saturation. For this reason these 2 extinction coefficient spectra give a very similar resulting curve with a maximum value of $9 \cdot 10^4$ at 492 nm, however, $(0.05)\ \frac{mmol}{l}$ yields a lower peak value of $5 \cdot 10^4$, caused by the falsified data of the A molecule in saturation. Therefore, the peak height is reduced and does not respond in a traceable and meaningful result. Consequently, the concentration of the A molecule dissolved in pH 9 were chosen below $0.05\ \frac{mmol}{l}$.
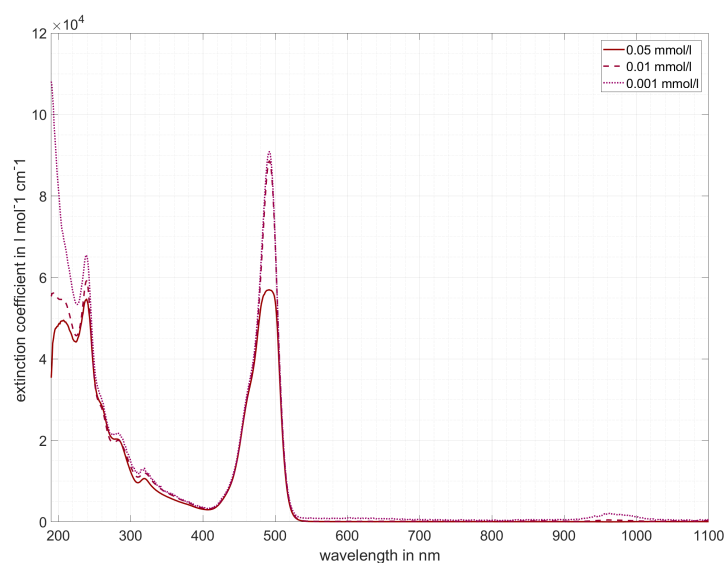
Figure 4.4: Extinction coefficient spectra of FTSC dissolved in pH 9 depicted in a series of 3 different concentrations $(0.05, 0.01, 0.001)\ \frac{mmol}{l}$.

After conducting the spectral overlap of the area normalized D emission spectrum (blue) and the background corrected A extinction coefficient spectrum (red), the Förster distance R_0 was determined. Figure 4.5 shows one example of the recorded fluorophore spectra with the resulting overlap spectrum (green). For the reason of 3 different intensity scales, the D emission as well as the A extinction scale were assigned to the left and right tinted in red and blue. The overlap function was area normalized, otherwise it would not be possible to arrange all 3 spectra into 1 single graph. However, the peak maximum is itemized to picture the relation of the magnitudes and counts around $6.5 \cdot 10^{13} \ nm^4 mol^{-1} cm^{-1}$
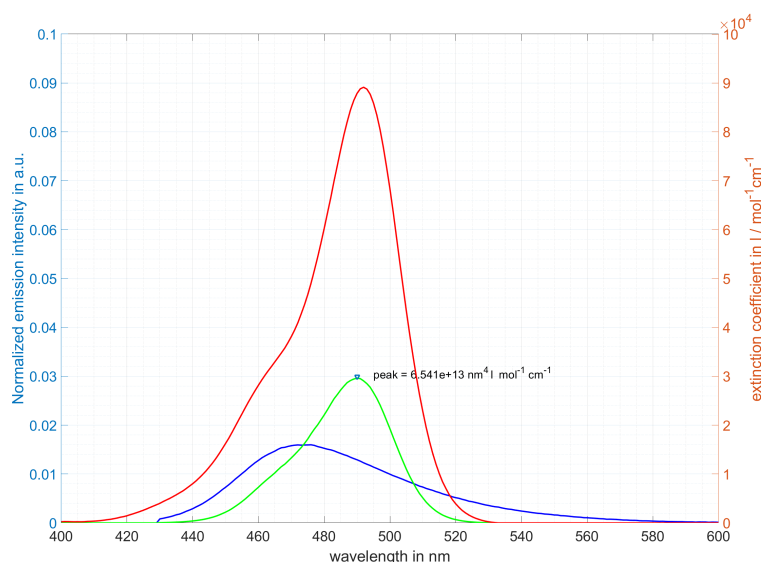
Figure 4.5: This figure includes 2 axis. The blue axis shows the donor corrected emission and the red axis depicts the acceptor extinction coefficient spectrum. In order to graph the overlap function (green) in the same figure, it was area normalized.

In figure 4.6 the colored curves show the resulting Förster distance calculations of different concentration compositions between D and A, depicted on the ordinate. The D concentration was held to 0.0005 $\frac{mmol}{l}$ but the D

and A compound ratios, here 1 : 1, 1 : 2, 1 : 5 and 1 : 10, were regulated by the A concentration, with the meaning 1 part D and 10 parts A, as it is displayed at the latter ratio. On the abscissa the interval variations of the base line correction is laid. 12 different steps were carried out to classify the relevance of the base line determination. Since the spectra data was not manipulated, small deviations can be seen in each curve. However, the variations of the 12 increments only affects the 2nd digit of the Förster distance calculation measured in nm. This data series results in a Förster distance of $R_0 = (4.42 \pm 0.01)\ nm$, which appears to be plausible.
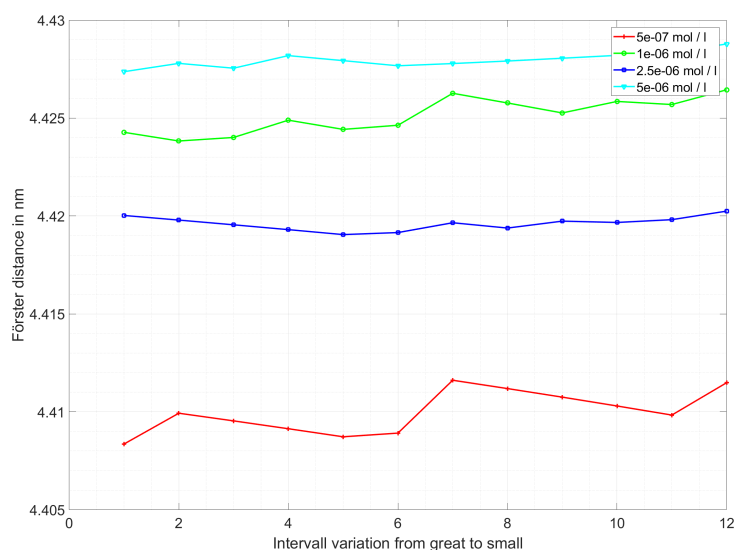
Figure 4.6: Calculated Förster distance of different concentration compositions between D and A.

The extinction coefficient measurements at an excitation wavelength $\lambda_{ex} = 400\ nm$ for different concentrations of D and A fluorophores dissolved in pH 9 yield for both into a converging exponential slope, depicted in figure 4.7. To visualize the deviation of the very small concentrations, an exponential fitting model was used and applied to the data, depicted as green dotted

lines.

Generally, the extinction coefficient is a molecule specific figure of merit including the excitation wavelength and the environment dependency. However, at very low or high concentrations this key figure can not be calculated correctly and diverges, in this example from $0.002 \cdot 10^{14} \frac{mmol}{l}$ downwards. Although there is a lack of data points towards higher concentrations, both graphs give an overview of the extinction coefficient tendency.
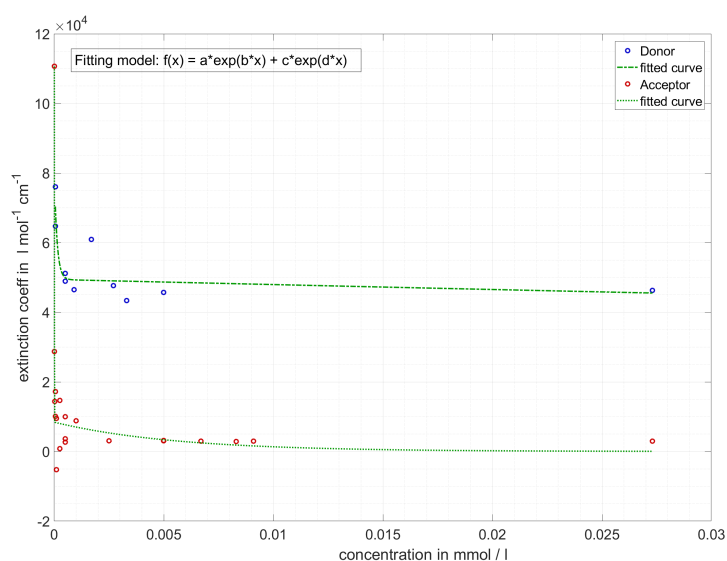
Figure 4.7: Extinction coefficient development (green line) of donor and acceptor fluorophore dissolved in pH 9. Single values were evaluated at an excitation wavelength of 400 nm in dependence of the concentration.

As already mentioned in section 2.2, RET takes place in the range up to 10 nm. Following figure 4.8 shows the dependency between Förster distance R_0 and the A concentration increase of the ratio measurement series. Once again, the data point cloud was sloped with a fitting model function, with the goal to show the Förster distance development. Besides the outliers at

very low concentrations, marked with arrows, the data points even out at around 4.4 *nm*.
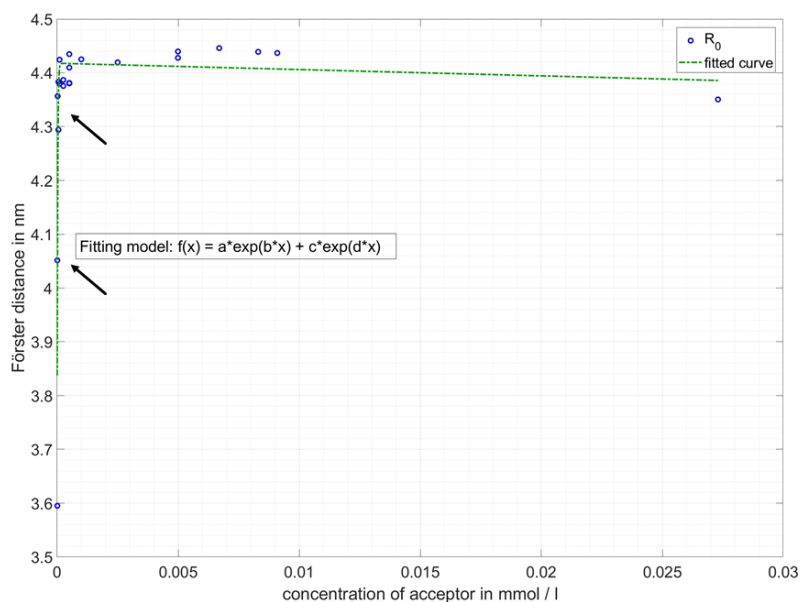
Figure 4.8: Evaluation of the Förster distance R_0 in dependence of the acceptor concentration of the donor-acceptor composite. The tendency is shown with the help of an exponential function.

4.2 FRET efficiency

Once the Förster distance was determined, taking notice, that it is a compound specific figure of merit, the FRET efficiency was worked out through the donor quenching and the acceptor sensitization, see figure 4.9. According to [10], both outcomes, η_D and η_A need to be equal or nearly equal and greater than zero to be able to constitute a RET with the possibility of a fluorescence observation. Further, D quenching is not enough to prove

the process of RET, as quenching can be caused by other mechanisms than the trivial D intensity deactivation. For this reason, the RET from D to A with a subsequent fluorescence of the latter needs to be measured following an excitation of the D.

Clarifying the difference on this occasion : donor quenching results in decreasing luminescence intensity caused by any form of deactivation, whereas the A sensitization states the intensity change in presence of the D species, after excitation by radiation, weighted by the ratio of the extinction coefficients measured at the excitation wavelength.
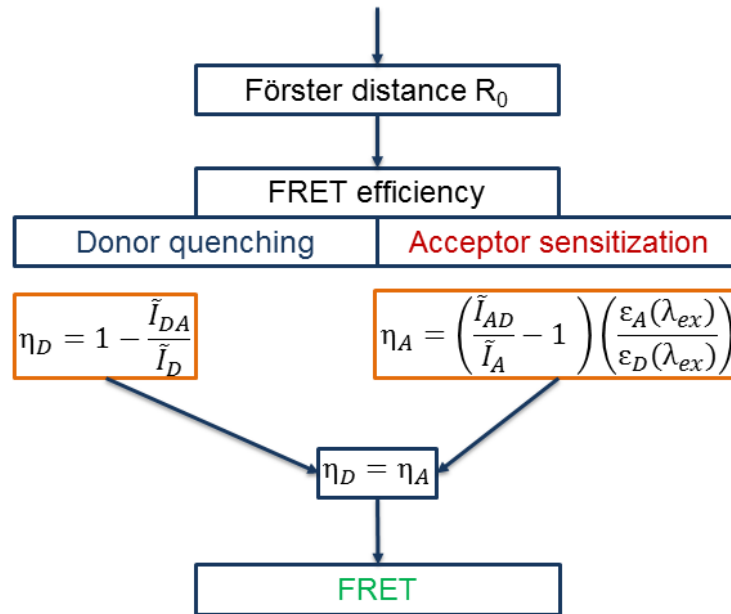
Figure 4.9: Block diagram illustrating the determination of the FRET efficiency.

4.2.1 Mixed signal observation

In the course of data evaluation, the recorded D-A mixed spectra of different fluorophore concentrations were analyzed. To identify the amount of exag-

gerated emitted fluorescent energy, id est quenching of the donor and an acceptor sensitization, pure signal spectra of D and A were used to model the recorded mixed signal spectrum. The goal was to find a multiple of the measured pure D and A spectra, to determine how much the mixed signal changed due to quenching and sensitization. With the help of the equations in section 2.3, bullet **3.** the concentrations of D and A were calculated as part of the mixed D-A compound solution. Subsequently these concentrations were produced and the emission spectra were recorded, defined as $\vec{I}_D$ and $\vec{I}_A$.

Figure 4.10 illustrates a theoretical composition of the pure D and A emission spectra, which result in the mixed D-A spectrum, when summed up. Instead of fitting a multidimensional polynomial function to the mixed signal, the pure D and A emission spectra (previously obtained) were used to determine the weighting variables C_1 and C_2. These factors C_i helped adjusting the pure fluorophore signal spectra (blue and red) to the mixed signal spectrum, illustrated in figure 4.11 (dashed black line).
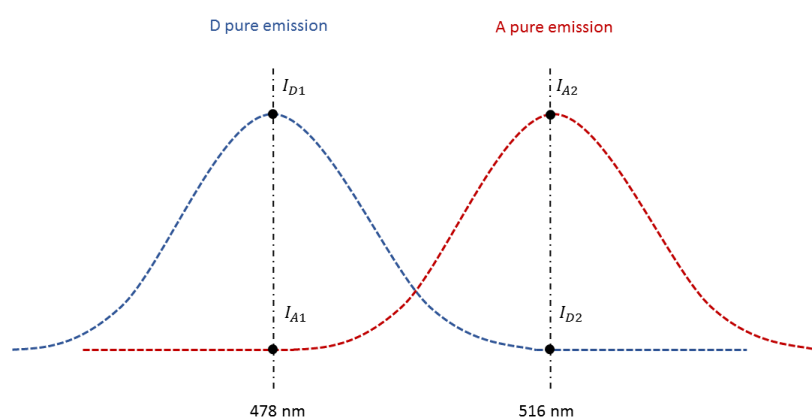
Figure 4.10: Theoretical overlap of pure donor and acceptor emission spectra.

Due to the fact, that the overlap, more specifically the outliers of the single spectra intrude into the other species spectrum, there is an interrelationship between both pure spectra marked at the maximum emission intensities 478 nm and 516 nm. Id est, the spectra were reduced to the very minimum of 2 representable points, $I_{D1,2}$ and $I_{A1,2}$, which scale with the calculated weighting factors C_1 and C_2.

Following equations 4.1 and 4.2 deal with the derivation of the weighting factors C_i to formulate the recorded D-A mixed signal $\vec{I}_{MIX}$. I_{DA} and I_{AD} express the fluorescence intensities relatively to the fluorophores of D or A in presence of A or D (subscript DA or AD).

$$C_1 \cdot \vec{I}_D + C_2 \cdot \vec{I}_A = \vec{I}_{MIX}$$
$$with$$
$$C_1 I_{D1} + C_2 I_{A1} = I_{DA}$$
$$C_1 I_{D2} + C_2 I_{A2} = I_{AD}$$

(4.1)

Using equation 4.1 C_1 and C_2 can be derived as follows:

$$C_1 = \frac{I_{AD} - C_2 I_{A2}}{I_{D2}}$$
$$and$$
$$C_2 = \left(I_{DA} - \frac{I_{AD} I_{D1}}{I_{D2}} \right) \cdot \frac{I_{D2}}{I_{A1} I_{D2} - I_{A2} I_{D1}}$$

(4.2)

Having said that figure 4.11 depicts the theoretical mixed signal of a D-A solution, it also illustrates the expected D quenching and A sensitization. The peak intensities are likely to rise with increasing the fluorophores concentration. But the fluorescence needs to predominate the intensity height change, in order to ensure a positive sensing of a prior RET. The initial state

is displayed in dashed lines and the RET mechanism is indicated by the arrows, which show the de-and increase of the cumulated black line.

Finally the factors $C_{1,2}$ were used to scale the pure D and A spectra and calculate the cumulated $\tilde{I}_{DA}$ and $\tilde{I}_{AD}$, shown in the diagram 4.9, to determine the FRET efficiencies η_D and η_A. Additional to the acceptor sensitization efficiency definition, both extinction coefficient values $\epsilon_{D,A}(\lambda_{ex})$ of D and A at the excitation wavelength $400\ nm$ were considered.
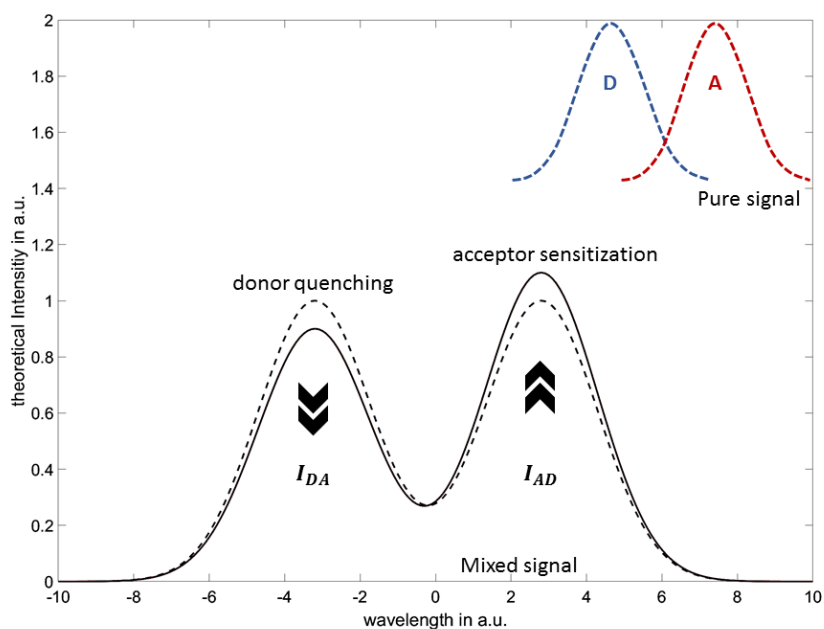
Figure 4.11: Theoretical donor-acceptor mixture emission spectrum (–). The peaks display the donor intensity spectrum in presence of the acceptor (subscript DA) and the acceptor emission intensity in presence of the donor (AD). At the same time the effect of donor quenching as well as acceptor sensitization is shown (-).

4.2.2 The extinction coefficient

The extinction coefficients $\epsilon_i(400)$ of both fluorophores dissolved in pH 9 at 400 nm are presented in figures 4.12 and 4.13. Besides the outliers, because of the very low concentrations such as $5 \cdot 10^{-9} \frac{mol}{l}$ (e.g. the red curled curve in figure 4.13), the extinction coefficient values at the predetermined wavelength measure around $4.4 \cdot 10^4 \frac{l}{mol \; cm}$ for the D and $0.1 \cdot 10^5 \frac{l}{mol \; cm}$ for the A fluorophore. All concentration depicted in the tables on the right side, which do not deviate apparently from the average, are marked with a black bracket.
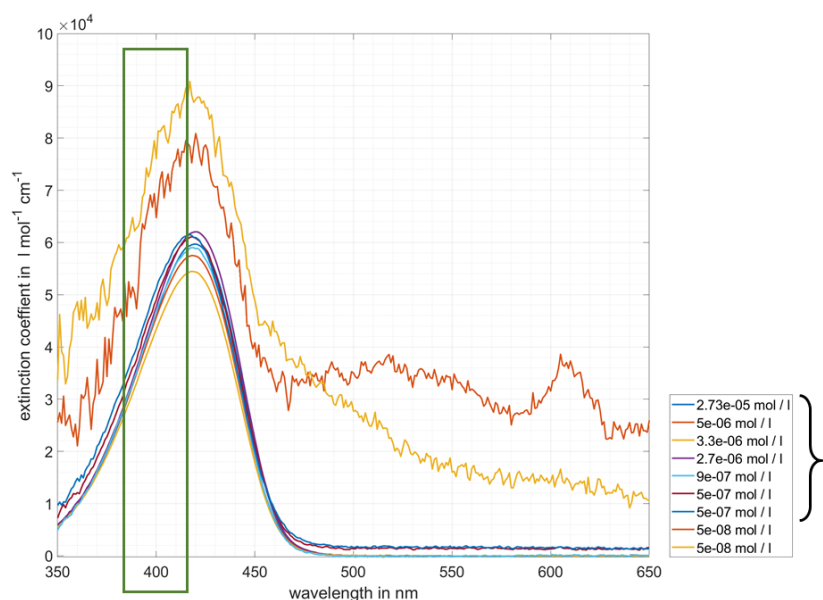
Figure 4.12: Extinction coefficient spectra of different donor concentrations. 400 nm marking at the excitation wavelength.
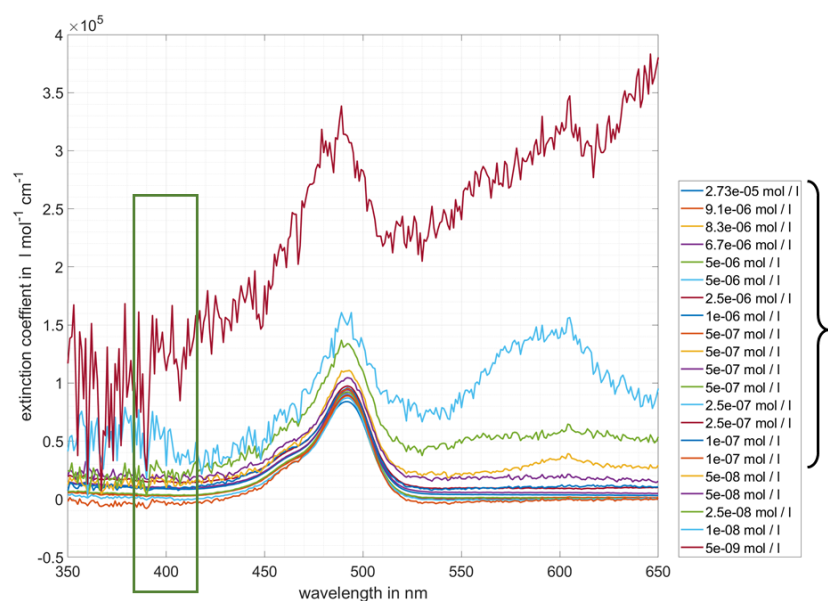
Figure 4.13: Extinction coefficient spectra of different acceptor concentrations. 400 *nm* marking at the excitation wavelength.

Figure 4.14 illustrates the difference between the recorded mixed signal (red) and the pure, cumulated spectrum (blue) with the intensity on the ordinate and wavelength on the abscissa. To emphasize once again, both spectra compilations were recorded using the same D or A concentrations with the same equipment settings, either for the mixed or pure spectra. So the same concentrations of the D and A fluorophores, which were set up in different ratios as D-A mixture, were replicated as pure solutions.

This example shows a D-A compound ratio of 1 : 1 with the concentration of 0.0005 $\frac{mmol}{l}$. On the left side at the maximum D emission intensity of 478 *nm*, the pure signal is some counts higher than the mixed signal. Different situation at the right peak at 516 *nm*, the mixed spectrum lies below the cumulated spectrum in blue.

Part of the same batch of concentration series ($c = 0.0005 \frac{mmol}{l}$), but in a different ratio, is shown in figure 4.15. Here the proportions are set to 1

part D and 10 parts A $(1 : 10)$. On the left side, the intensity difference is more pronounced with about 20 counts, in comparison to the previous example on the right side, the pure signal is 40 counts higher than the mixed intensity. Additionally, a bathochromic shift in the range of $[515 - 520]\ nm$ is noticeable at the A emission peak with rising ratio.
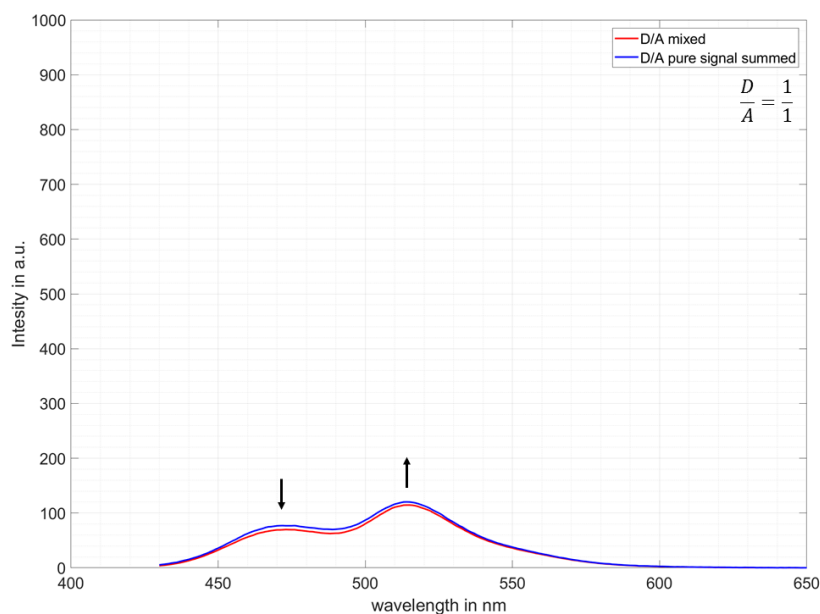
Figure 4.14: Donor-Acceptor pure (blue) and mixed (red) signal with a compound ratio of $1 : 1$ and the concentration basis $0.0005\ \frac{mmol}{l}$.
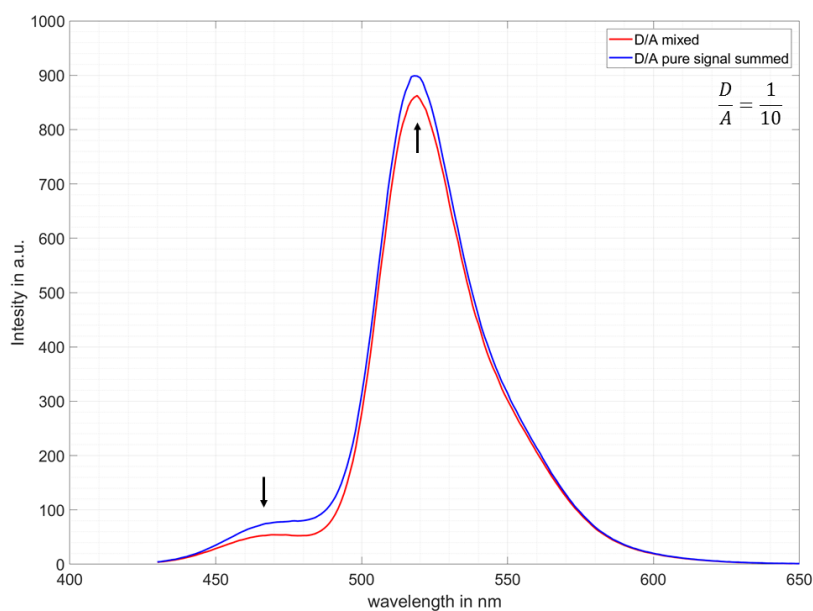
Figure 4.15: Donor-Acceptor pure (blue) and mixed (red) signal with a compound ratio of 1 : 10 and the concentration basis 0.0005 $\frac{mmol}{l}$.

Both examples in figure 4.14 and 4.15, part of a seven-piece series, demonstrate how the D as well as the A emissions behave with a mutual concentration ratio change showing their emission intensity evolution at the same instrument settings.

4.2.3 Donor quenching and acceptor sensitization

According to equation 2.14 and equation 2.15 the D quenching as well as the A sensitization were calculated, leading to efficiency values in the range of $[0, 1]$.
With growing A concentrations up to a ratio of 1 : 10 the efficiency reaches nearly 0.35, appearing to be a positive quenching, depicted in figure 4.16.

However, the A sensitization does not show any increase through out the different ratio variants. Hence, both RET efficiency determinations do not show any similarities - $\eta_D \neq \eta_A$.
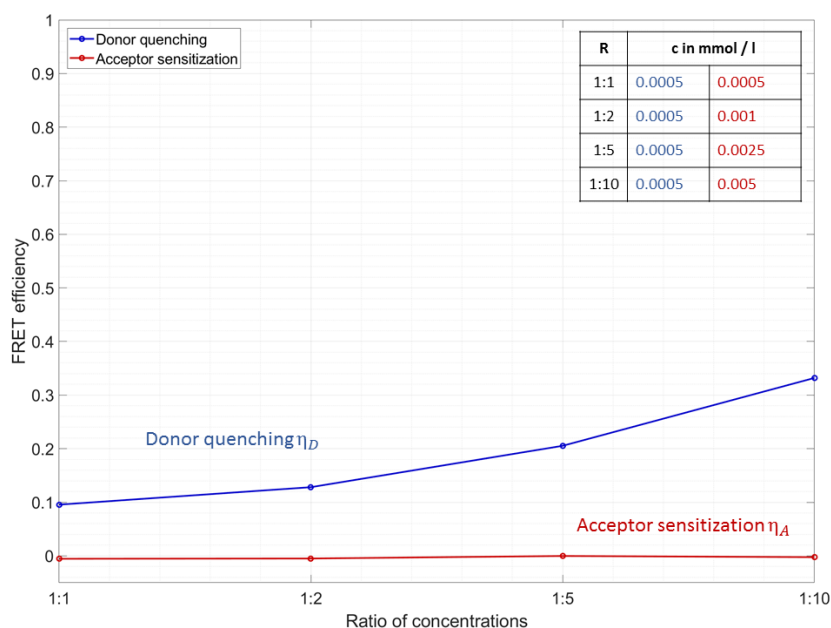
Figure 4.16: Donor quenching and acceptor sensitization with the ratios $1 : Z$, $Z \in [1, 2, 5, 10]$ and the donor basis concentration of $0.0005 \frac{mmol}{l}$.

Figure 4.17 shows a positive A sensitization at a D-A ratio of 10 : 1 with given concentration values in the table. Due to the very low concentrations in the range of a few nanomol, the FRET efficiency calculations were falsified with the result of an A sensitization of around 0.4 counts. Referring to the extinction coefficient spectra of both fluorophores in figure 4.12 and figure 4.13, the molecule solution concentrations lower than the magnitude of $10^{-7} \frac{mol}{l}$ returns an incorrect response at the efficiency calculations. Hence, the efficiency values up to the ratio of 1 : 1 can mislead the interpretation. Besides the outliers, both efficiency calculations do not resemble each other or show a similar tendency, so that there is no apparent evidence of a RET

between the D and the A fluorophore in the solution pH 9.

Figure 4.16 and figure 4.17 demonstrate an increasing D quenching, but no A sensitization at any stage of the investigation. The D quenching is necessary but not sufficient to be prove a successful RET between the D and A fluorophore.

R	c in mmol / l	
10:1	5E-05	5E-06
5:1	5E-05	1E-05
2:1	5E-05	2.5E-05
1:1	5E-05	5E-05
1:2	5E-05	1E-04
1:5	5E-05	2.5E-04
1:10	5E-05	5E-04
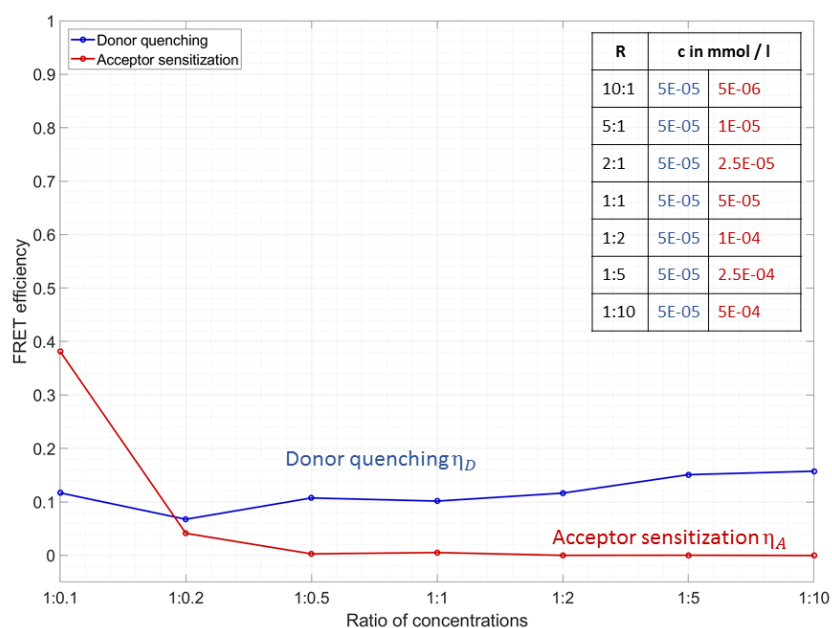
Figure 4.17: Donor quenching and acceptor sensitization with the ratios $1 : Z$, $Z \in [0.1, 0.2, 0.5, 1, 2, 5, 10]$ and the donor basis concentration of $0.00005 \frac{mmol}{l}$.

5 Capillary $d = 0.4\ mm$

In order to get more insight into higher solution concentrations, referring to the limitation caused by the width of the standard quartz glass cuvette (see figure 3.8), it was considered to modify the investigation method. To overcome the constrain of the receptacle dimensions, several experiments were carried out. The investigation process remained the same, but various cuvette substitutes were tested one by one in the running order as follows: standard quartz glass cuvette, synthetic material cuvette with a base area of (10 x 5) *mm*, standard NMR tube and a glass capillary with a diameter of 0.4 *mm*, cited in section 2.3.2.

The synthetic cuvette with the rectangular base area was not able to fulfill the purpose of downsizing the interaction volume and the inner filtering effects could not be minimized. Although the incident light beam irradiates the probe perpendicular to the edge of 0.5 *cm*, it nevertheless travels the same length when using a square based cuvette 1 *cm*, vice versa when coming from the broadside.
Another idea was to use a NMR tube with a cylindrical shape. Even though the diameter was apparently smaller than the standard cuvette, it was not enough to measure a noticeable difference to the measurements up to now. So both of these investigation methods were rejected.
In the end the capillary was chosen for the final investigation experiments on fluorophores dissolved in pH 9. It was thin enough to avoid inner filtering

effects, easy to be integrated into the existing set-up and quickly to purchase.

Due to the lack of a proper capillary fixture, I have defined a new set-up depicted in figure 5.1. A capillary tube (CAP; section 2.3.2) was centered vertically in the cuvette (CUV) with a conic piece of plastic (AT), which fitted into the aperture of the cuvette and served as an adapter between both components. To prevent the CAP of slipping through the plastic attachment in the CUV, a very thin hose of plasticine (black mark) was wrapped around the CAP, as shown in the side view of the figure. In order to hinder the CAP from tilting, it had to be fixed at the bottom side directly on the specimen holder of the spectrofluorophotometer. That is the reason why the CUV had no bottom (dashed line). After the CAP was centered to the CUV, it was adjusted so the specimen could be fully irradiated by the light beam and the spectra measurements could be performed as supplied earlier in this work.
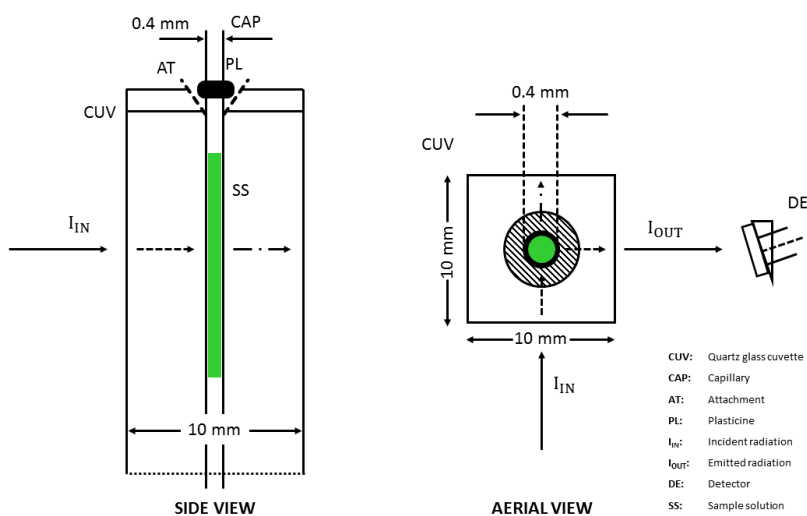
Figure 5.1: Assembly of capillary cuvette set-up.

The following 2 figures, 5.2 and 5.3, illustrate the results of the measurements with the capillary implemented into the cuvette. For these recordings both fluorophores were prepared in saturated solutions.

The first figure shows the results of the D fluorophores excitation and emission spectra, but they were executed at different instrument settings. Between 400 nm and 450 nm a small excitation peak is visible. As already discussed, it differs from the cited specifications, the most because of the different solvent. However, the D emission spectra at different excitation wavelengths do not show the same slopes. At an excitation wavelength of 400 nm the emission peak measures its maximum at 478 nm, which goes equal with the measurements done with the standard quartz glass cuvette and a similarity is observable. Regarding the violet tinted curve, the emission spectrum's maximum deviates very largely from the others, because its excitation wavelength at 333 nm is far away from the maximum excitation wavelength (423 nm).

In comparison to the D excitation and emission peaks in figure 5.2, the A data spectra are well defined in the range of $(400\ to\ 600)\ nm$, see figure 5.3. In this example, the spectra data, which is recorded with the same settings, is marked with a dotted line. Additionally, this relationship is signed with brackets in the given legend in the figure. As can be seen, the A emissions spectrum maximum (516 nm; orange doted line) is received by exciting at 493 nm (blue dotted line). Further various emission spectra are depicted, which show the difference of the intensity height according to their corresponding excitation wavelength. All excitation wavelengths below $\lambda_{EX} = 400\ nm$ (yellow, violet, green, light blue and red line) yield into an intensity signal between 100 and 200 counts. The reason for this low outcome is the character of the excitation spectrum. From nearly 250 $nm to$ 400 nm the excitation intensity makes up about 5% of its maximum value at 493 nm. Compared to that, the emission spectrum originating from $\lambda_{EX} = 460\ nm$ (blue line) measures 900 counts at 516 nm, although it was not excited with the peaks maximum wavelength. Thus, the best emission yield would be

obtained with $\lambda_{EX} = 493\ nm$.
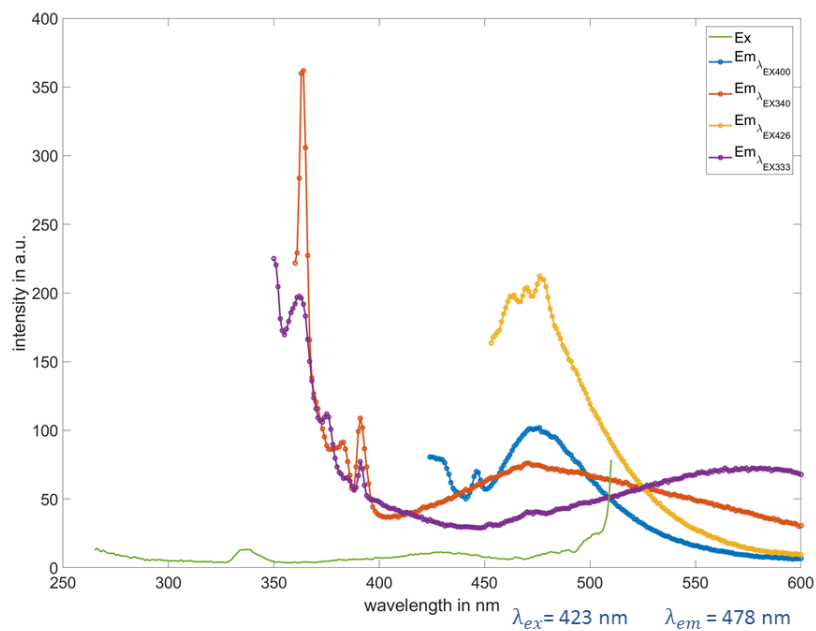
Figure 5.2: Donor excitation and emission spectra at saturation concentration of $0.14\ \frac{mmol}{l}$ recorded with the capillary set-up.
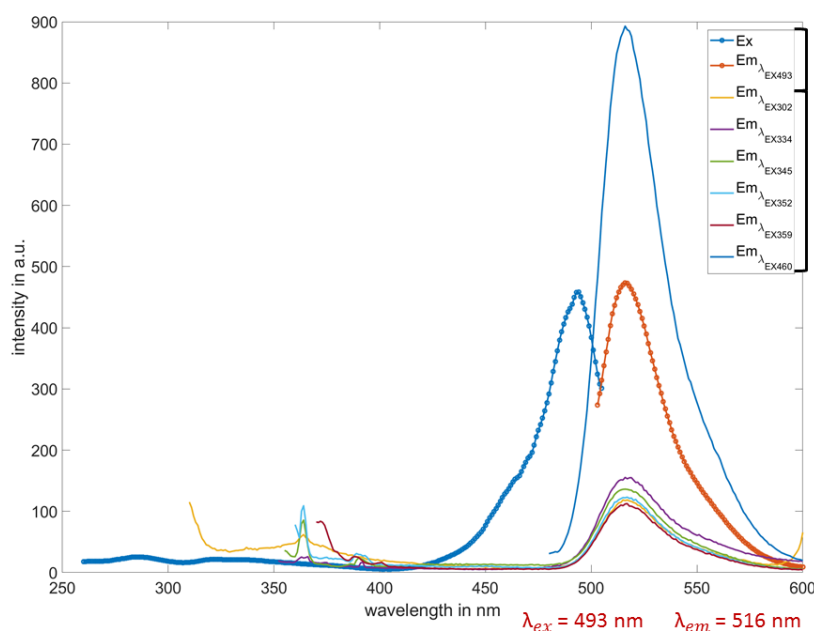
Figure 5.3: Acceptor excitation and emission spectra at saturation concentration of 0.3 $\frac{mmol}{l}$ recorded with the capillary set-up.

With this extra investigation method, using the thin capillaries, the highest possible concentrations, the saturation concentrations of both fluorophores dissolved in pH 9, were measured avoiding inner filtering effects. The results in figure 5.2, without any clear excitation and emission peak, could be caused by the utilized saturation concentration and the fact that the composition is in form of colloidal particles in an aqueous environment. In comparison to that, the A fluorophore shows smooth excitation and emission peaks.

At this point, after all given tasks accomplished and the expired time plan, the project research concerning this master thesis was finalized.

6 Discussion and perspectives

The target of this diploma thesis was to find a method to investigate 2 predefined fluorophore molecules dissolved in DMF and pH 9 and determine the Förster distance and the [F]RET efficiency, which were designated figures of merit.

For this purpose, 3 working steps were performed:

First, the solubility of the fluorophores *7-(Diethylamino) coumarin-3-carbohydrazide* (DCCH) assigned as donor and *Fluorescein-5-thiosemicarbazide* (FTSC) as acceptor molecule was studied by recording transmittance spectra. The distilled water at pH 9 was prioritized, according to preliminary assumptions, although the results of the solutions in DMF appeared informative. Therefore DMF was rejected and instead the alkaline solvent was preferred in the course of investigation. The reasons lied above all in the lack of information about the impact of the solvent DMF on the fiber-fiber conjunctions, which were to be studied in collaboration with a doctoral thesis.

Second, proceeding with the solvent pH 9, the Förster distance was determined to $R_0 = 4.4$ *nm* of the predetermined molecule pair with fluorescence characteristics following the calculation of the overlap integral $J(\lambda)$ using the area normalized donor emission spectrum and the acceptor extinction coefficient spectrum.

The third investigation step was to find the correlation between donor quenching and acceptor sensitization, to identify the [F]RET efficiency. Both of them did not resemble one another. Hence, the outcome of the current investigation led to a temporary conclusion, that the solvent environment

of pH 9 is not suitable for this predefined fluorophore pair.

6.1 Lessons learned

Most of the key issues which emerged, can be traced back to the interplay of 3 essential parameters: the **fluorophore molecular structure**, the prepared **solutions** in dependence of the **concentrations**.
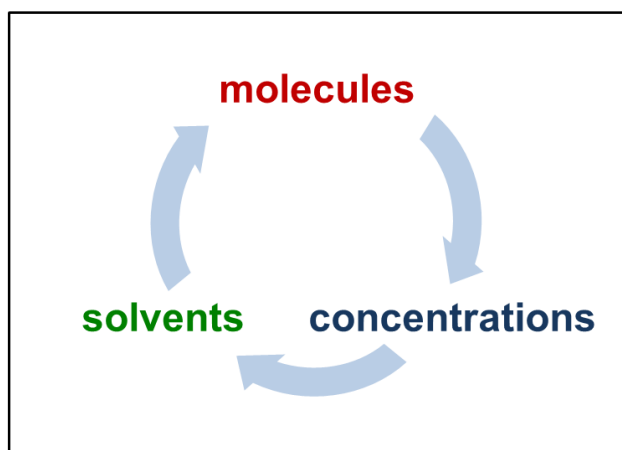
Figure 6.1: The 3 essential parameters.

1. **Acquire a suitable donor-acceptor pair**
   [11], Both fluorophores need to operate in the same spectral range. But moreover, they need to provide a spectral overlap. Although a spectral overlap is a requirement, it is not sufficient to obtain a positive result in the [F]RET efficiency. The greater the spectral overlap $J(\lambda)$ between donor and acceptor, the higher is the resulting value of the Förster distance R_0 (e.g. acceptors with large extinction coefficient spectra). Assuming the overlap is in compliance with the requirements, the

quantum yield turns out to be highly relevant. Small errors on the quantum yield of the donor Φ_D do not have a major impact on the calculations of R_0, since it is related as the sixth root (increasing Φ_D by the factor of 2 the Förster distance value R_0 shows a deviation of $\pm 12\%$). However, drastic changes in quantum yield can have influence on the outcome, since this variable is proportional to the fluorescence intensity.

Figure 6.2 illustrates the donor and the acceptor emission with the same recording properties (concentration $c = 0.1 \frac{mmol}{l}$, excitation wavelength $\lambda_{EX} = 400$ nm, ambient conditions and device settings (slit width: 1.5 high[1])). It shows a significant difference between both emission intensity heights, which vary by a factor of around 11.

According to the scientific paper (Lingliang Long et al., 2015 [12]) a coumarin based fluorophore, very similar to the one used in this work, has a quantum yield of $\Phi_D = 0.184$. In relation to that, quinine sulfate (0.1 M H_2SO_4) has a quantum yield of 0.58 and fluorescein (0.1 M $NaOH$) surpasses with 0.95 [11], respecting the different solvents these fluorophores were dissolved in.

Nonetheless, this contrast, referring the coumarin and the fluorescein based molecules utilized in this work, could lead to the conclusion of a low donor quantum yield in relation to the quantum yield of the acceptor. One reason for the low emission intensity could be self-quenching effect, caused by the rotation of the N-N bond of the hydrazide group. Another possibility for the low fluorescence yield could be solubility of the chromophore coumarin in the solvent. In comparison to the donor, the acceptor is operating verifiably good in the alkaline environment (pH 9).

---

[1]The slit width scales from 1 to 20, by starting with a closed aperture. "high or low" represents the intensity scaling. "High" responds into 100% intensity, corresponding to the raw data. "Low" was set to result in 50% intensity height.
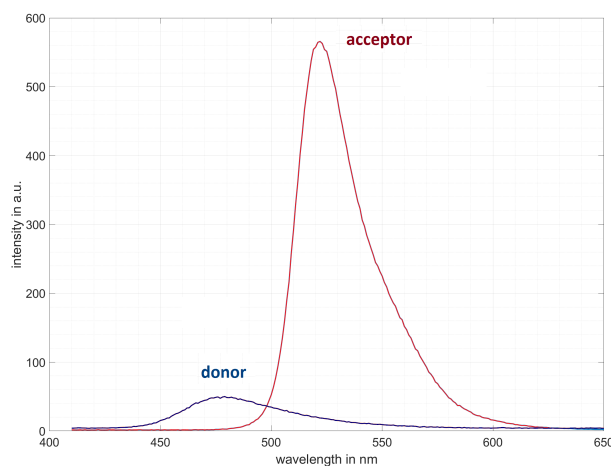
Figure 6.2: Donor and acceptor emission spectra recorded with the same conditions.

2. **Find an appropriate solvent**

Referring to the investigation results, FTSC is soluble in water (pH 9) and has a relatively high solubility in DMF. In comparison to that, the donor fluorophore is not recommended to be used in water at pH 9, comparing the intensity heights in figure 6.2. Despite starting experiments of dissolved donor and acceptor fluorophores in DMF, following investigation steps were canceled, in order to continue with the solvent pH 9.

Observing the molecular structures of the fluorophores (figures 2.19a and 2.19b) more in detail, insights could lead to new perceptions.

Aromatic molecules are generally very stable and do not react very easily with other substances. Hydrogen bound to carbon atoms, especially to aromatic molecules, is not likely to interact with an aqueous environment at pH 9. But primary and secondary amines, carboxylic and hydroxy groups interact with the alkaline solvent and by means of the acid dissociation formulation, the functional groups can be deprotonated.

In the case of the donor molecule, which is built up from a cumarin

chromophore in the basis, with a diethylamine and an acylhydrazine attached to it. The latter can lose its hydrogen atoms in an alkaline solvent. The acceptor molecule, with a fluorescein chromophore in the basis consists of 2 secondary amines and 1 primary amine in conjunction with a sulfur atom. Besides the fact, that the carboxylic group will be deprotonated in pH 9, it contributes with the hydroxy group to a water solubility. Comparing both fluorophores, the donor molecule does not possess these functional groups and thus, the solubility in water at 300K is very poor.

Summarized, the chromophores with their functional groups are strongly dependent on their environment (solubility, polarity or viscosity et al.) and can be a trigger for de-/protonation. In the course of de-/protonation the molecular electronic structure can be altered, ergo, the optical behavior changes. For this reason, a deprotonation itself or in combination with an increase of the acceptor concentration could be the cause of a solvatochromism in the emission spectra in figure 3.9.

3. **Prepare the proper concentration**

In order to avoid inner filter effects, when measuring the fluorescence intensity, it is better to work at low optical densities, according to (J.R.Lakowicz, 2010 [11]), $OD = 0.05$.

When the investigation came down to high concentrations (solvent saturation), the standard quartz glass cuvette was exchanged by a capillary based set-up. Due to its smaller diameter, the reduced interaction volume, caused by the increasing concentrations and the high OD, fills out the capillary diameter, which lowers or remedies the inner filtering effect.

6.2 Conclusion and perspectives

According to the investigations, carried out in this master thesis, the system of fluorophores dissolved in pH 9 did not lead to an acceptor sensitized fluorescence following a resonant energy transmission (RET) between the donor and acceptor molecules.

Although, the aqueous solution at pH 9 was not suitable for the donor, it could be interesting to investigate the spectroscopic behavior of different fluorophores in a measurement series of various solvents and additionally changing the pH value.

Beside the fact that, as indicated in the discussion, both fluorophores need to be dissolvable in the same solvent, the dependence on the solvent could be used to learn more about the bonding mechanisms of cellulose fibers. Assuming that the fibers are soaked with a solvent different of an aqueous based one, for example DMF, the contribution of the fiber-fiber conjunctions through hydrogen bondings could be hindered or minimized. In consequence the role of the other forces such as Coulomb, Van der Waals or mechanical interlocking could get more relevant, when investigating the force behavior between interlinked fibers.

Quenching effects different from the one resulting in RET falsify the interpretation of the outcome. There are various quenching types described in this thesis. In addition to these, oxygen needs to be taken into consideration. Solvents with enriched oxygen can strongly influence the outgoing signal as a quencher. The amount can be reduced by bubbling the solution with an inert gas such as argon or nitrogen. Another way to extract the oxygen out of the solution could be a temperature treatment with simultaneously enhancing the molecule movement.

The donor molecule dissolved in pH 9 played an essential role in denying a RET to the acceptor molecule. Apart from third-party effects, the donor quantum yield, similar to the utilized fluorophore, was adopted from a pa-

per as quoted in the master thesis. Hence, in order to minimize the impact of prescribed variables such as the orientation factor κ^2, the donor quantum yield ϕ_D and the refractive index n of the fluorophore in their environment, investigations should be established and specific factors that determine the quality of these variables should be accounted for.

In respect of the accounting complexity, I recommend to start the research with a profound fluorophore pair in a suitable environment, in a liquid or solid state. Within sensing the distance between interconnected fibers applying a spectroscopic investigation method based on FRET, the fluorophores: 1st need to be attachable to the cellulosic fibers, 2nd dissolvable in a solvent, which is compatible to both, the fluorophores themselves and the fibers and 3rd have a high quantum yield.

Appendix

Bibliography

[1] Peter Rückert, Sandra Hodecek, and Emanuel Wenger. *The History of Paper and Watermarks from the Middle Ages to the Modern Period. Bull's Head and Mermaid*. The Bernstein Project Booklet of the exhibition. Gulde-Druck GmbH Tübingen, 2009. ISBN: 978-3-00-026752-9. URL: http://www.bernstein.oeaw.ac.at/twiki/pub/Main/ProjectExhibitions/bernstein_2009_book_en.pdf (visited on 2018) (cit. on p. 1).

[2] Jonathan M. Bloom. *Papermaking: The Historical Diffusion of an Ancient Technique*. 2017. Chap. 3. URL: https://link.springer.com/content/pdf/10.1007%2F978-3-319-44654-7_3.pdf (visited on 2018) (cit. on p. 1).

[3] Matheus Poletto, Vinícios Pistor, and Ademir J. Zattera. *Structural Characteristics and Thermal Properties of Native Cellulose*. Ed. by Theo van de Ven and Louis Godbout. InTech, 2013. Chap. 2. DOI: 10.5772/50452. URL: https://www.intechopen.com/books/cellulose-fundamental-aspects/structural-characteristics-and-thermal-properties-of-native-cellulose (visited on 2018) (cit. on p. 2).

[4] D. Klemm et al. *Comprehensive Cellulose Chemistry Volume l. Fundamentals and Analytical Methods*. WILEY-VCH Verlag GmbH Weinheim, 1998. Chap. 2. ISBN: 3-527-29413-9 (cit. on pp. 2, 3).

BIBLIOGRAPHY

[5]   U. Hirn and R. Schennach. *Comprehensive analysis of individual pulp fiber bonds quantifies the mechanisms of fiber bonding in paper*. Apr. 2015. URL: https://www.nature.com/articles/srep10503 (visited on 2018) (cit. on pp. 4, 5).

[6]   U. Hirn et al. *THE AREA IN MOLECULAR CONTACT IN FIBER-FIBER BONDS*. Graz University of Technology et al. URL: https://www.researchgate.net/profile/Ulrich_Hirn/publication/264200347_The_Area_of_Molecular_Contact_in_Fiber-Fiber_Bonds/links/54f6b4c00cf27d8ed71e7bc8/The-Area-of-Molecular-Contact-in-Fiber-Fiber-Bonds.pdf (visited on 2018) (cit. on pp. 4, 5).

[7]   Frederik Weber. "Viscose fibre - a model system to investigate the influence of charges on the properties of handsheets and fibre-fibre joints." Doctoral thesis. Graz University of Thechnology, 2014 (cit. on p. 5).

[8]   Stefan Bienz et al. *Spektroskopische Methoden in der organischen Chemie*. 9th ed. Georg Thieme Verlag, 2016. ISBN: 978-3-13-576109-1 (cit. on pp. 10–12, 22).

[9]   Alexander Tovstopyat. "Photophysical properties of new conjugated molecules." Doctoral thesis. Graz University of Thechnology, 2016 (cit. on pp. 10, 14).

[10] Igor Medintz and Niko Hildebrandt. *FRET - Förster Resonance Energy Transfer. From Theory to Application*. 2014th ed. Wiley-VCH, 2010. ISBN: 978-3-527-32816-1 (cit. on pp. 13, 22, 25, 27–29, 31–33, 78).

[11] Joseph R. Lakowicz. *Principles of Fluorescence Spectroscopy*. 3rd ed. Springer, 2010. ISBN: 978-0-387-31278-1 (cit. on pp. 15–22, 25, 27, 28, 31–34, 36–38, 60, 95, 96, 98).

[12] Lingliang Long et al. *A fluorescent probe for hypochlorite based on the modulation of the unique rotation of the N–N single bond in acetohydrazide.* 2015. URL: http://pubs.rsc.org/-/content/articlelanding/2015/cc/c5cc03972j#!divAbstract (visited on 2018) (cit. on pp. 32, 96).

[13] L. Stryer. "Fluorescence Energy Transfer as a Spectroscopic Ruler." In: *Annual Review of Biochemistry* 47:819-846 (1978). URL: https://www.annualreviews.org/doi/pdf/10.1146/annurev.bi.47.070178.004131 (visited on 2018) (cit. on p. 28).

[14] Th. Förster. "Zwischenmolekulare Energiewanderung und Fluoreszenz." In: *Annalen der Physik* 437 (1-2 1948), pp. 55–75. URL: https://onlinelibrary.wiley.com/doi/abs/10.1002/andp.19484370105 (visited on 2018) (cit. on p. 28).

[15] R.M. Clegg. "Fluorescence resonance energy transfer." In: X.F. Wang and B. Herman. *Fluorescence imaging spectroscopy and microscopy*. Wiley, 1996, pp. 179–252. ISBN: 9780471015277 (cit. on p. 31).

[16] *Elektronenspektroskopie-Spektroskopie im ultravioletten und sichtbaren Spektralbereich*. ETH Zürich. Sept. 2011. URL: http://www.analytik.ethz.ch/vorlesungen/biopharm/Spektroskopie/UV.pdf (visited on 2018) (cit. on p. 35).

[17] W.Gootwald and K.H.Heinricht. *UV/VIS-Spektroskopie für Anwender. Die Praxis der instrumentellen Analytik herausgegeben von U.Gruber und W.Klein*. Wiley-VCH, 1998. ISBN: 3-527-28760-4 (cit. on pp. 39, 40).

[18] Shimadzu Corporation. *Spectrofluorophotometer RF-5301PC Series*. Instruction Manual. Shimadzu Corporation Analytical and Measuring Instrument Division, 2008 (cit. on pp. 41, 42).

[19] *7-(Diethylamino)coumarin-3-carbohydrazide*. SIGMA-ALDRICH now Merck. Mar. 2018. URL: https://www.sigmaaldrich.com/catalog/product/sigma/36798?lang=de&region=AT (visited on 2018) (cit. on pp. 43, 45).

[20]   *Fluorescein-5-thiosemicarbazide*. SIGMA-ALDRICH now Merck. Mar.
       2018. URL: https://www.sigmaaldrich.com/catalog/product/
       sigma/46985?lang=de&region=AT (visited on 2018) (cit. on pp. 44,
       45).

[21]   *di-Sodium tetraborate decahydrate*. SIGMA-ALDRICH now Merck. May
       2018. URL: https://www.sigmaaldrich.com/catalog/product/mm/
       106308?lang=de&region=AT (visited on 2018) (cit. on p. 49).

[22]   Jr. Workman Jerry and Lois Weyer. *Practical Guide to Interpretive Near-
       Infrared Spectroscopy*. Crc Pr Inc, 2007. ISBN: 978-1584885948 (cit. on
       p. 61).